

Early Ediacaran lichen from Death Valley, California, USA

GREGORY J. RETALLACK

Department of Earth Sciences, University of Oregon, Eugene, Oregon, 97403–1272, U.S.A.
Email: gregr@uoregon.edu

(Received 14 September, 2022; revised version accepted 02 December, 2022)

ABSTRACT

Retallack GJ 2022. Early Ediacaran lichen from Death Valley, California, USA. Journal of Palaeosciences 71(2): 187–218.

Enigmatic tubestones from the basal Ediacaran Noonday Formation of southern California have been interpreted as fluid escape structures or as stromatolites in a “cap carbonate”, created by marine precipitation at the termination of Snowball Earth glaciation. However, doubts about this interpretation stem from permineralized organic structures within the tubes with hyphae and attached spheroidal cells, and thallus organization comparable with lichens. These “tubestones” are here named *Ganarake scalaris* gen. et sp. nov. The fungus was aseptate as in Mucoromycota and Glomeromycota, and the spheroidal photobiont has the size and isotopic composition of a chlorophyte alga. The tubes are most like modern window lichens (shallow subterranean lichens) and formed nabkhas (vegetation-stabilized dunes) of a loess plateau comparable in thickness and extent with the Chinese Loess Plateau of Gansu. Loess paleosols of three different kinds are recognized in the Noonday Formation from geochemical, petrographic, and granulometric data. The Noonday Formation was not a uniquely Neoproterozoic marine whitening event, but calcareous loess like the Peoria Loess of Illinois and Chinese Loess Plateau of Gansu.

Key-words—Lichen, Nabkha, Loess, Cap carbonate, Ediacaran, California.

INTRODUCTION

NEOPROTEROZOIC tillites overlain sharply by dolostone on many continents, such as the Noonday Formation over Kingston Peak Formation in Death Valley, California (Fig. 1), have long been recognized as “strange bedfellows”, an abrupt change from glacial tillites to tropical marine carbonates implying as much as 45°C temperature rise (Hoffman, 2011). Hypotheses for formation of cap carbonates in the ocean include increased oceanic alkalinity from enhanced continental weathering, oceanic overturn, gas hydrate destabilization, a flood of meltwater on the ocean, sediment starvation, or enhanced microbial activity (Yu *et al.*, 2020). Boron and calcium isotopic studies add difficulties, such as a depression then rise in world ocean pH of 1.1, which is more than an order of magnitude increase in hydronium ion activity (Kasemann *et al.*, 2005, 2010; Ohnemüller *et al.*, 2014). Strontium, zinc and magnesium isotopes and iodine/alkaline earth ratios also are evidence for continental weathering or meltwater enhanced to an unparalleled degree in “cap carbonates” (Kunzmann *et al.*, 2013; Liu *et al.*, 2014; He *et al.*, 2020). These extremes are envisaged as termination

of a global glaciation without subsequent analog, called Snowball Earth (Kirschvink, 1991; Hoffman *et al.*, 1998). Neoproterozoic cap carbonates also contain distinctive carbonate shrubs attributed to marine microbes (Fraiser & Corsetti, 2003), and “tubestones” regarded as water escape (Cloud *et al.*, 1974), gas escape (Kennedy *et al.*, 2001; Bosak *et al.*, 2010), or unusual stromatolite structures (Corsetti & Grotzinger, 2005).

Tubestones of the Neoproterozoic Noonday Formation and their biological significance are one topic of this study (Fig. 2), but so is an alternative non-marine interpretation of cap carbonates as terrestrial loess (Retallack, 2011, 2021), rather than whittings of global marine carbonate precipitation (Hoffman, 2011). Extreme pH changes of more than an order of magnitude hydronium activity in the world ocean are literally unbelievable, but normal for different soil horizons (Retallack & Burns, 2016; Lukens *et al.*, 2018). Partly silicified tubestones of the Noonday Formation examined in petrographic thin sections, scanning electron microscope, and by palynological preparation now reveal a variety of complex permineralized organic structures in tubestones here assigned to a new genus and species of fungus, *Ganarake scalaris*.

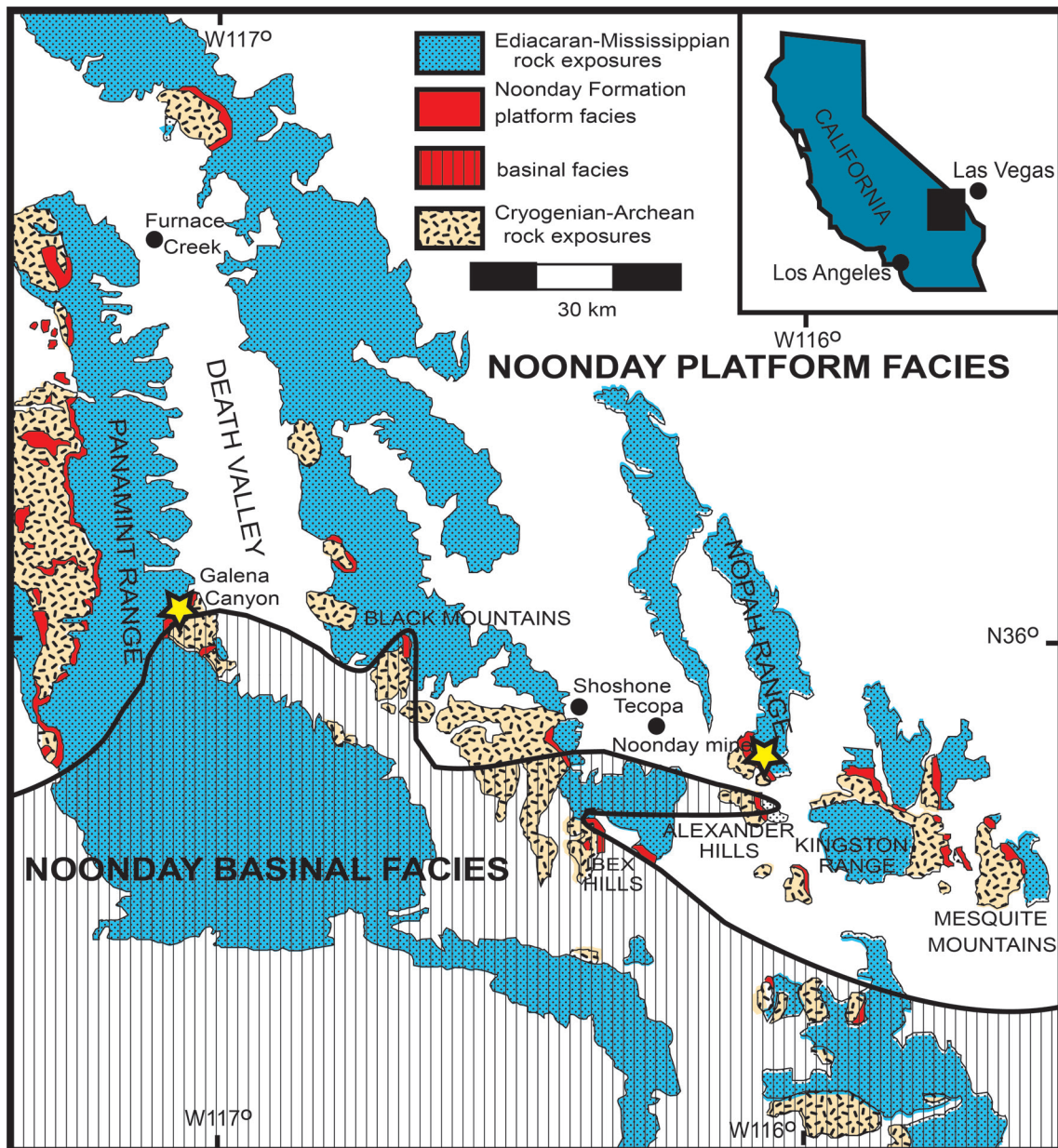


Fig. 1—Noonday Formation distribution and sample sites in Galena Canyon and Noonday Mine, showing intraformational erosional lowland–basinal and upland–platform facies (data from Wright *et al.*, 1976).

Lichenized fungal features of *Ganarake* and a variety of petrographic and geochemical observations now challenge previous marine interpretations of the Noonday Formation.

GEOLOGICAL BACKGROUND

The Noonday Formation, 60–400 m thick (Williams *et al.*, 1974), sharply overlies tillites of the Kingston Peak Formation in the Death Valley region (Fig. 1), and is conformably overlain by shale and carbonate of the Johnnie

Formation (Fig. 3). It used to be called “Noonday Dolomite” (Williams *et al.*, 1974), and that is the dominant mineral of the upland–platform facies, but the basinal Radcliff Member is heterolithic: only 20 m thick of red arkose in the platform facies, but 200 m of grey and red breccia, sandstone, shale, and dolostone within the basinal facies (Pettersen *et al.*, 2011, 2013). Radcliff Member is a replacement term of Pettersen *et al.* (2011) for “Ibex Formation” (Corsetti & Kaufman, 2003, 2005), which fills 200 m of paleorelief to the south (Creveling *et al.*, 2016). Below the Radcliff Member on the upland–

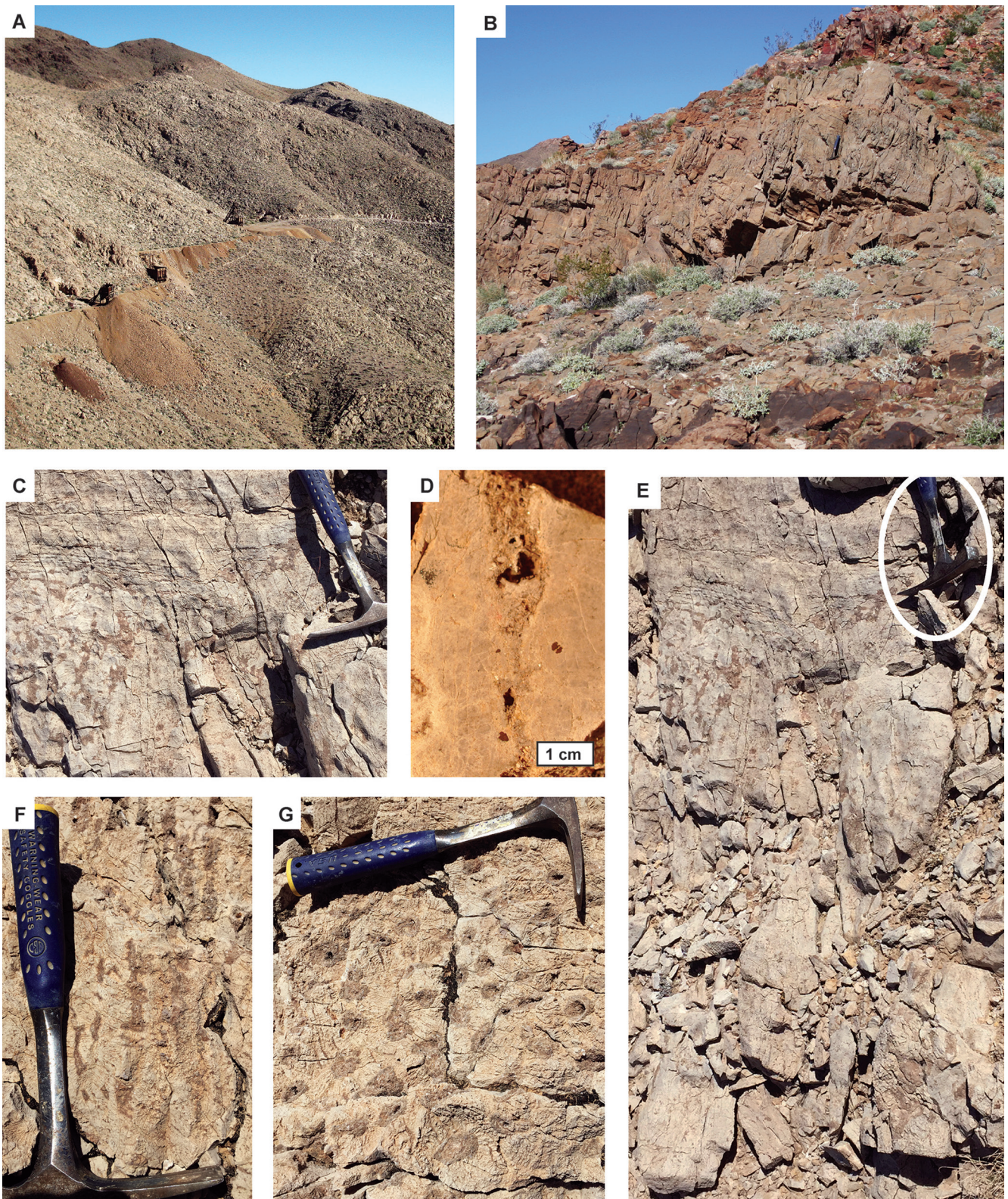


Fig. 2—Noonday Formation outcrops. (A) measured section near Noonday Mine; (B) upper part of formation with silicified tubestones in Galena Canyon; (C–E) tubestones; (C) upper part of tubestone unit truncated by bedded dolostone without tubestones; (D) polished slab with accordion like flanges and waists of a tube; (E) vertical tubes of Pahuntoi bed truncated by and overlying layers without tubes; (F) vertical view of tubestone; (G) horizontal view of tubestone.

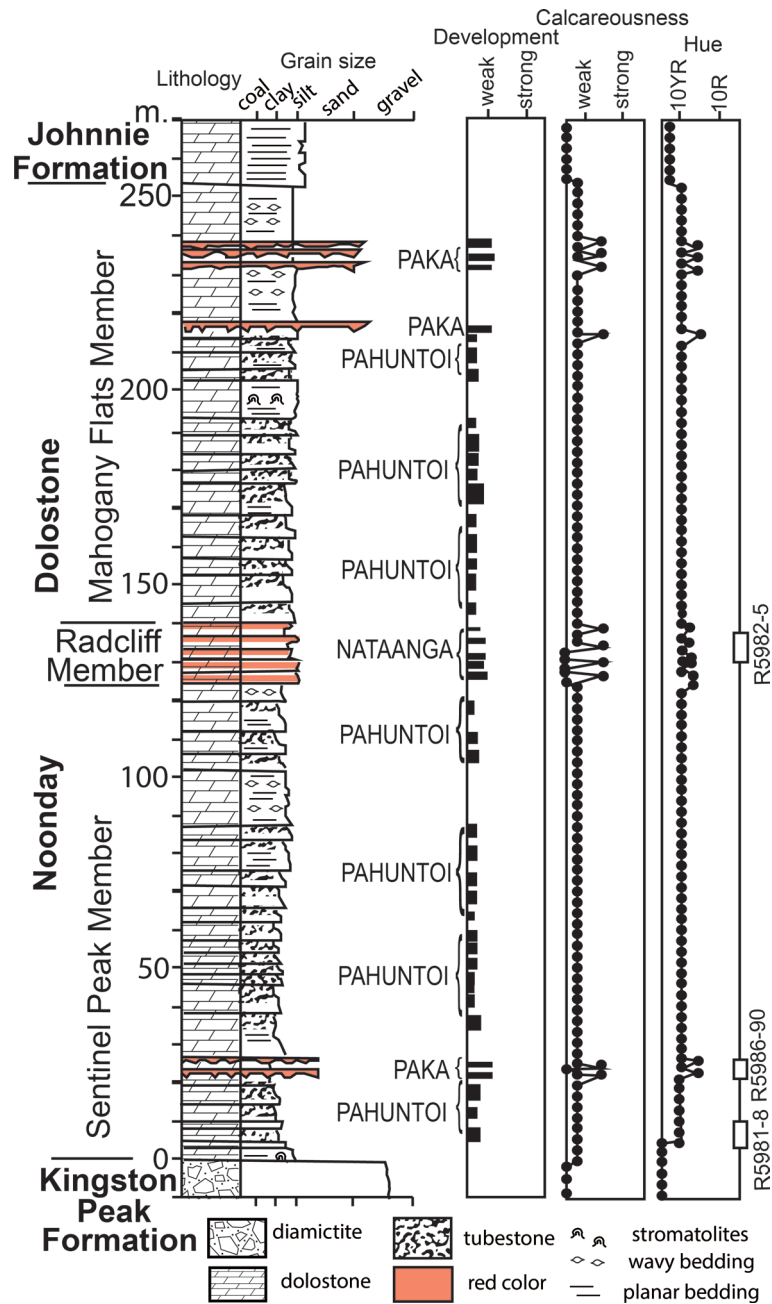


Fig. 3—Measured section of the Noonday Formation near Noonday Mine, showing identified paleosols and their development, calcareousness, and Munsell color hue. Paleosols were named using words for pipe (Pahuntoi), fragment (Paka) and orange (Nataanga) in the Shoshoni Native American language (Shoshoni Language Project, 2019).

platform facies is the Sentinel Peak Member and above the Radcliff Member is the Mahogany Flats Member (Pettersen *et al.*, 2011), also with numerous beds of tubestones (Fig. 3).

Geological dating of the Noonday Formation is insecure because inferred from international correlation with other “cap carbonates”, representing sea level and chemostratigraphic anomalies, but with several alternative interpretations (Xiao & Narbonne, 2020). Kingston Peak Formation tillites and sea-

level low-stand have been correlated with the last Cryogenian glacial advance, often called Marinoan (Prave, 1999; Kennedy & Eyles, 2021), but should be called the Elatina Glaciation (Williams *et al.*, 2008). The golden spike for the base of the Ediacaran Period has been driven into Nuccaleena Formation, a “cap carbonate” overlying tillites of the Elatina Formation in Enorama Creek, South Australia (Knoll *et al.*, 2006). Another “cap carbonate” overlying tillite is the lower Doushantou

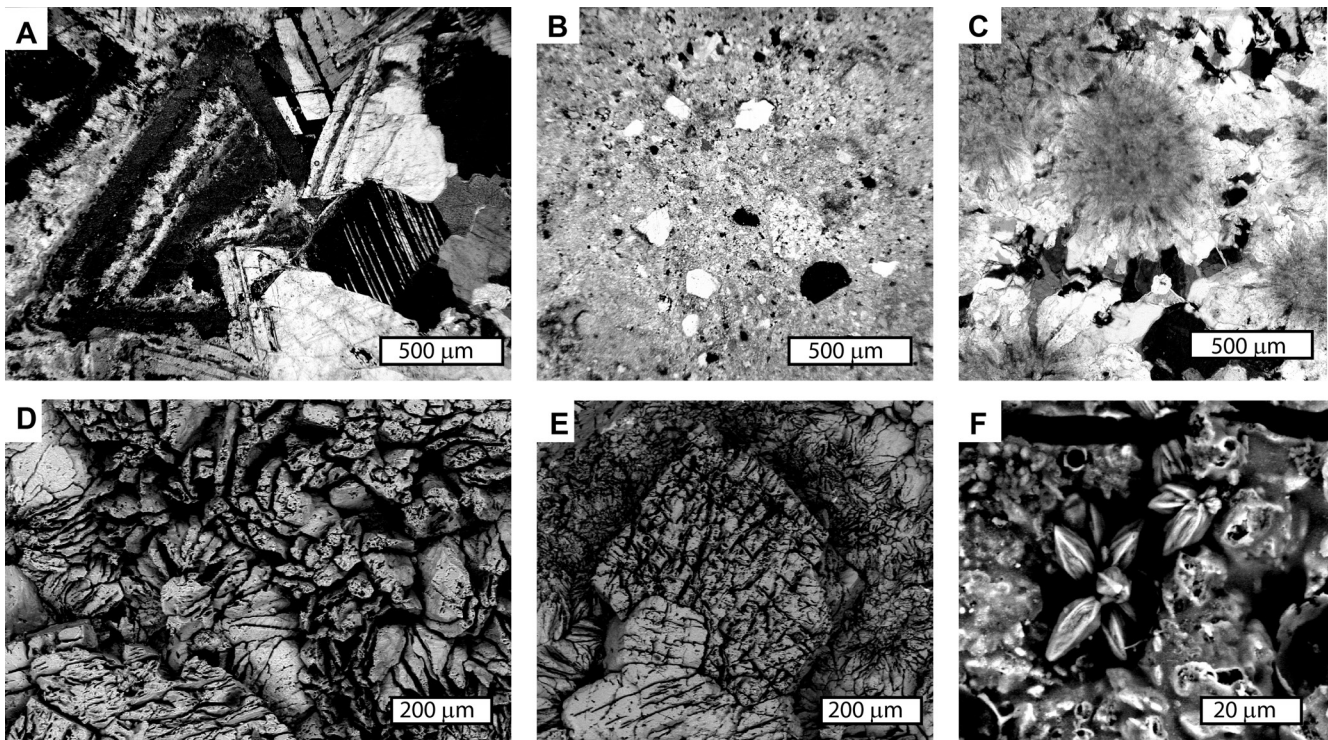


Fig. 4—Petrography of Noonday Formation in thin section (A–C) and scanning electron microscope images in back scatter mode (D–F). (A) central fill of tubestone, dolomite after calcite spar; (B) quartz, feldspar and rock fragments in matrix of dolomitic silt; (C) needle fiber dolomite after calcite in cavity fill sparry dolomite; (D) central fill of dolomite spar (lower left), cavity lining dolomite, and dolomite–quartz–feldspar silt (upper right); (E) rounded dolomite rhomb; (F) bipyramidal skeletal dolomite after whewellite. Specimen numbers in the Condon Collection of the Museum of Natural and Cultural History, University of Oregon are F116110C (A, C–E), R5988 (B), and F116110A (F).

Formation, which includes volcanic tuff dated at 634.57 ± 0.88 Ma U–Pb by ID–TIMS (isotope dilution thermal ionization mass spectrometry) on zircon (Zhou *et al.*, 2019). Other dates by the same method are 635.2 ± 0.6 Ma in the basal carbonate of the Doushantou Formation, 632.5 ± 0.5 Ma for the upper carbonate, and 551.1 ± 07 Ma for uppermost shale and phosphorite of the Doushantou Formation (Condon *et al.*, 2005). Between the two lowest dated horizons is a paleokarst recording low sea level, and the Doushantou Formation contains another paleokarst level higher in the section and below a tuff dated by the same method at 599.3 ± 4.2 Ma (Barfod *et al.*, 2002; Gan *et al.*, 2021). Each of the Doushantou paleokarsts correspond with transient low $\delta^{13}\text{C}$ isotopic values of carbonate labelled EN1 and EN2 (Xiao & Narbonne, 2020). There are two different views on why the isotopic anomalies in “cap carbonates” might be correlative globally: (1), they are caused by global oceanic geochemical anomalies such as methane release (Kennedy *et al.*, 2001); (2), they are due to paleokarst weathering, sometimes labelled “meteoric diagenesis” (Retallack *et al.*, 2021a). Chinese “cap carbonates” and isotopic anomalies are dated by four available dates (Barfod *et al.*, 2002; Condon *et al.*, 2005; Zhou *et al.*,

2019; Gan *et al.*, 2021) as 635.2 Ma for EN1 and either 602 or 580 Ma for EN2 (Xiao & Narbonne, 2020). Comparable age of the Noonday Formation comes from U–Pb ID–TIMS date of $< 651.7 \pm 0.6$ Ma within the Kingston Peak Formation, 110 m below the contact with the Noonday Formation (Nelson *et al.*, 2020), and paleomagnetic correlation and recognition of the *ca.* 565 Ma Shuram–Wonoka $\delta^{13}\text{C}$ excursion in the Rainbow Member of the Johnnie Formation, 490 m above the base of the Noonday Formation (Minguez *et al.*, 2015). Thus, the Noonday Formation is likely early Ediacaran (*ca.* 635 Ma) in age, as previously correlated (Corsetti & Kaufman, 2003).

Plate tectonic reconstructions show that southeastern California was equatorial during the Ediacaran, on the northern margin of an east–west oriented Laurentian Craton (Torsvik & Cocks 2013; Scotese, 2021). Paleolatitude of the Ediacaran Johnnie Formation has been estimated from paleomagnetism as $1^\circ \pm 4^\circ$, and the Cryogenian Kingston Peak Formation as $8^\circ \pm 4^\circ$ (Evans & Raub, 2011). Detrital zircon and Nd isotopic data reveal derivation of Noonday Formation quartzofeldspathic components from Proterozoic granitic rocks with mean ages of 1400 and 1675 Ma (Lang Farmer & Ball, 1997; Mahon *et al.*, 2014).

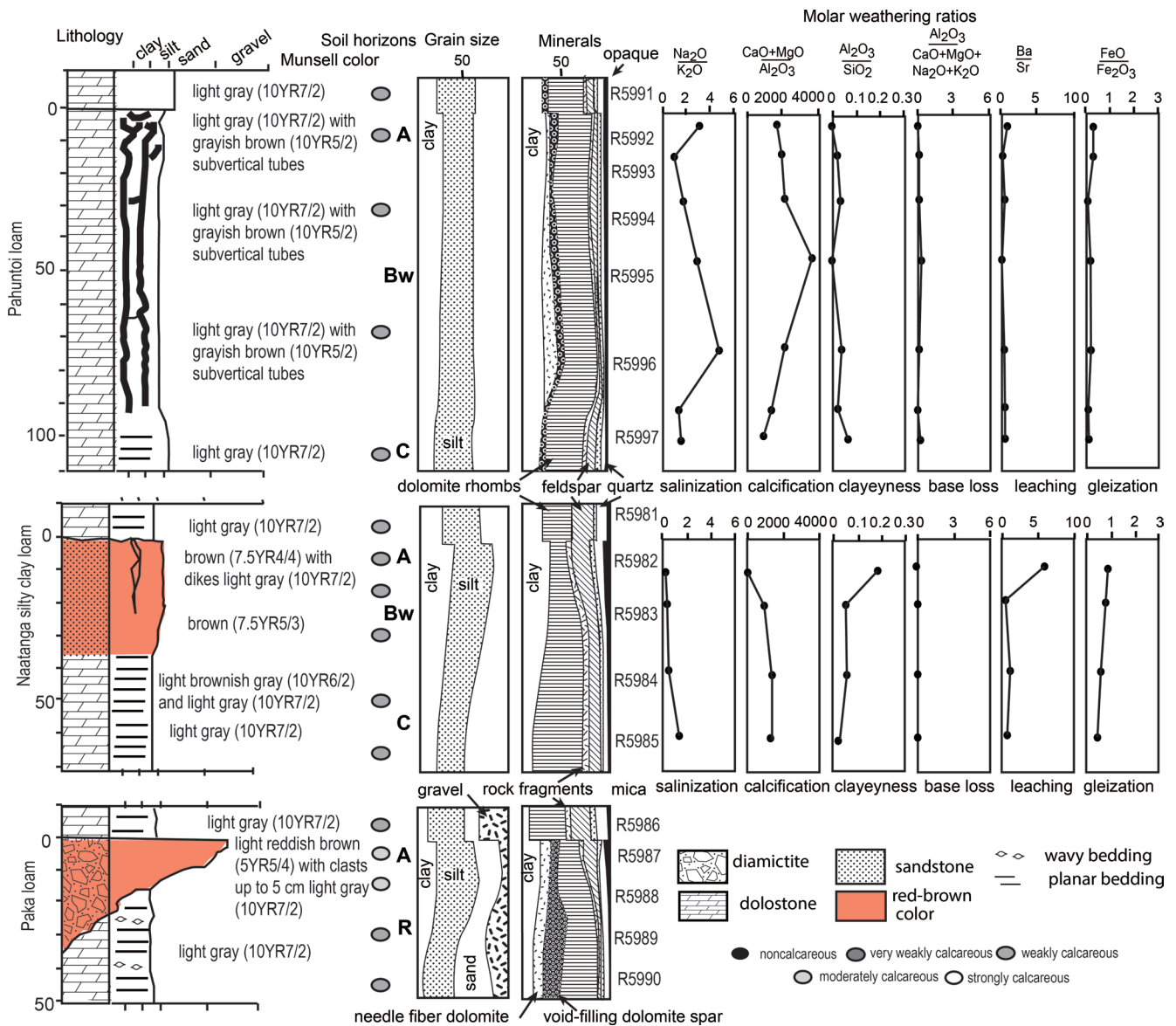


Fig. 5—Petrographic and geochemical data on Noonday Formation beds near Noonday Mine, California. Data displayed includes Munsell hue, calcareousness determined by acid application (0.1M HCl), grain size and mineral composition determined by point counting petrographic sections, and molecular weathering ratios of major and trace elements determined by XRF analysis. Individual sampled levels are shown on Fig. 3.

Early diagenetic dolomitization of aragonite in the Noonday and other cap carbonates (Ahm *et al.*, 2019) is supported by observations of needle fiber fabric (Fig. 4C–F), typical of fungal aragonite (Verrecchia & Verrecchia, 1994; Bajnóczi & Kovács–Kis, 2006). Weathering by meteoric water is a classic explanation for dolomitization (Mehmoud *et al.*, 2018), and dolomite is catalyzed by microbial extracellular polysaccharides galactose and rhamnose favored by high CO_2 in soils (Zhang *et al.*, 2012; Kearsley *et al.*, 2012).

Folding created dips of 32° E on strike 264° near Noonday Mine (Fig. 2A), and 28° NW on strike 55° in Galena

Canyon (Fig. 2B). There is no evidence of pervasive late diagenetic potash metasomatism (Novoselov & de Souza Filho, 2015) with only traces of potash in dolostones, and even sandstones of the Noonday Formation have only 1.22–1.31 wt% K_2O . A Weaver index of illite crystallinity (ratio of 10/10.5Å peak in XRD trace) of 3.3 was determined for the Johnnie Formation near Noonday Mine (Retallack, 2020), and is compatible with burial by 3.4–4.4 km (Retallack, 2013). Observed overburden above the Noonday Formation is at least 6 km (Corsetti & Kaufman, 2003), with perhaps an addition 1.5 km of eroded Permian to Jurassic, shown in

the cross section for the southern Nopah Range including the Donna Loy Mine (Wernicke *et al.*, 1988). Burial compaction expected for 6.0–7.5 km burial can be calculated as 53–54 %, using a formula (Sheldon & Retallack, 2001) with 0.51 solidity, 0.49 initial porosity, and 0.27 fitting constant. Such compaction estimates are needed for paleoenvironmental interpretations and predict significant carbonate neomorphism and pressure solution (Bathurst, 1970; Wanless, 1979). Compaction was resisted in nodules and tubestones cemented by early diagenetic silica (Fraiser & Corsetti, 2003), as in other microfossiliferous Precambrian cherts (Knoll, 1985). The Noonday Formation was also locally affected by Mississippi Valley style lead–zinc mineralization from early Paleozoic migration of hydrothermal brines (Carlisle *et al.*, 1954; Church *et al.*, 2005). The Queen of Sheba Mine, 3 km southeast of the Galena Canyon outcrops examined for this study, is a replacement zone mainly of galena and chalcopyrite, 12 m thick and 123 m long, fed by faults and strata–concordant within a clearly defined sericitized and brecciated lower part of the Noonday Formation (Morton, 1965). The Noonday Mine is also below the measured section there, yet brecciation and mineralization were not observed within the measured section. Also in the region is polymetallic skarn mineralization associated with Cretaceous granitic intrusions (Newberry, 1987; Newberry *et al.*, 1991), also too localized to affect the sections examined here.

MATERIAL AND METHODS

Fieldwork

This study examined two localities in detail: (1), Galena Canyon in the Panamint Range (N 36.01988° W 116.9337° to N 36.020441° W 116.933569°), and (2), Noonday Mine in the southern Nopah Range (N 35.8219° W 116.09296° to N 35.822638° W 116.089111°). Geological sections were measured (Fig. 3), including detailed representative beds (Fig. 5). Samples from levels shown in Figs 3 and 5 are in the Condon Collection of the Museum of Natural and Cultural History of the University of Oregon. Field colors were determined by comparison with a Munsell Color Chart, and calcareousness by application of 0.1 molar HCl from an eye–drop bottle. Moderately calcareous (1–5% calcite) rocks form a white drop with audible bubbles, but weakly calcareous (dolomite, or < 1% calcite) rocks form very few bubbles (Retallack, 1997).

Distinctive, repeated bed types in the Noonday Formation were named Pahuntoi, Paka and Nataanga, using words for “pipe”, “fragment”, and “orange” in the Shoshoni Native American language (Shoshoni Language Project, 2019). Pahuntoi profiles are about 1 m thick, and consist of intervals of vertical tubestones petering out below, and abruptly overlain by bedded dolostone without tubestones (Fig. 2C, 2E). The tubestones are not continuous through the formation

but restricted within individual Pahuntoi levels (Fig. 3). Paka profiles are thin, red, dolostone breccias filling irregularly corroded cavities in underlying dolostone, and Nataanga profiles are cracked red sandstone with a lot of quartz and feldspar. One example of Pahuntoi and Nataanga profiles was selected for detailed petrographic and geochemical study, including point–counted proportions of sand, silt and clay, and of different mineral components, as well as rare earth element patterns and molar weathering ratios from major element analysis (Fig. 5). Paka profiles were not sampled because they were simple breccia fills of paleokarst without discernable internal horizonation. The most informative fossils described here from silicified Pahuntoi tubestones in Galena Canyon were from a stratigraphic level of 120 m, just below onlapping siltstones of Radcliff Member (Cloud *et al.*, 1974).

Laboratory studies

Samples were collected for geochemical analyses: trace elements by lithium borate fusion inductively coupled plasma mass spectrometry and major elements by atomic absorption spectroscopy with British Columbia granodiorite as a standard (Fig. 4). Ferrous iron was determined by Pratt titration, also by ALS Chemex, of Vancouver Canada. Petrographic thin sections were point counted for mineral composition and grain size using a Swift automated stage and Hacker Counting box. Both composition and size counts were 500 points, which has accuracy of 2% for common components (Murphy, 1983). Petrographic and chemical data is in Tables 1–4. Long axes of 1000 grains were measured for granulometric analysis using the Swift stage (Fig. 5), as in a comparable previous study (Retallack, 2011). Rare earth elements and yttrium (YREE) were normalized for Post–Archean Australian Shale (PAAS: Taylor & McLennan, 1985).

Three distinct techniques were used to prepare fossil specimens for microscopy. Standard thin sections were made of each kind of rock, and of especially promising silicified specimens. In another preparation, stock solution of HF was applied for 30 seconds, then rinsed off 25 times to etch the polished surface of a thin section billet, leaving organic remains in bas–relief for scanning electron microscopy in a QANTA environmental instrument in CAMCOR facility of the University of Oregon. Another method was standard palynological preparation by dissolution of the tubestones only, without matrix, in HF followed by 20 minutes of Schultz solution for mounting on slides for optical microscopy, and on stubs for scanning electron microscopy (Batten, 1999).

Nomenclature

The electronic version of this article in Portable Document Format (PDF) in a work with ISSN or ISBN represents a published work according to the International Code of Nomenclature for Algae, Fungi and Plants (Turland

Table 1—Chemical composition (wt %) from XRF of Ediacaran rocks from California.

Pedotype	Sample	SiO ₂	TiO ₂	Al ₂ O ₃	Fe ₂ O ₃	FeO	MnO	CaO	MgO	Na ₂ O	K ₂ O	P ₂ O ₅	SrO	BaO	LOI	Total	g.cm ⁻³
sandstone	5658	74.10	0.2	2.65	1.81	<0.01	0.26	5.92	3.14	0.02	1.23	0.27	0.05	0.04	8.32	98.01	2.5968
sandstone	5659	74.90	0.2	2.64	1.85	<0.01	0.26	6.00	3.29	0.02	1.22	0.27	0.05	0.05	8.32	99.07	2.6089
sandstone	5660	74.50	0.2	2.80	2.01	0.13	0.26	5.73	3.08	0.02	1.31	0.28	0.05	0.05	8.04	98.33	2.5937
sandstone	5661	76.10	0.24	2.79	1.94	<0.01	0.23	5.41	2.60	0.01	1.27	0.31	0.06	0.04	7.11	98.11	2.4095
sandstone	5662	79.70	0.25	2.89	2.02	0.33	0.19	5.48	1.19	0.02	1.25	0.30	0.05	0.04	5.71	99.09	2.5920
limestone	F110148	1.82	0.02	0.31	0.46	0.29	0.01	40.1	12.4	0.04	0.05	0.01	0.02	<0.01	44.3	99.54	not done
limestone	F123803	22	0.86	2.02	1.98	0.65	0.09	21.7	14.95	0.01	0.99	0.04	0.01	0.02	33.7	98.37	not done
Nataanga	R5982	2.45	0.02	0.74	1.6	0.52	0.21	30.3	19.75	0.01	0.22	0.04	0.02	0.19	44.7	100.26	2.2659
Nataanga	R5983	1.47	0.01	0.13	1.07	0.39	0.16	31.7	20.5	0.01	0.04	0.02	0.02	0.01	45.7	100.84	2.3268
Nataanga	R5984	0.71	0.007	0.08	1.08	0.26	0.16	31.1	20.3	0.01	0.04	0.02	0.01	0.03	46	99.51	2.3844
Nataanga	R5985	1.98	0.01	0.08	1.2	0.26	0.17	32.3	18.85	0.01	0.01	0.02	0.02	0.02	45.1	99.77	2.2631
Pahuntoi	R5992	1.35	0.007	0.06	0.2	0.11	0.06	30.9	21.6	0.02	0.01	0.02	0.01	<0.01	45.9	100.13	2.6064
Pahuntoi	R5993	1.69	0.007	0.06	0.24	0.12	0.06	30.7	21.3	0.01	0.02	0.02	0.01	<0.01	45.7	99.81	2.6484
Pahuntoi	R5994	0.76	0.007	0.05	0.18	0.13	0.06	30.7	21.5	0.01	0.01	0.02	0.01	<0.01	46.1	99.4	2.5115
Pahuntoi	R5995	1.72	0.007	0.03	0.2	0.13	0.06	30.5	21.3	0.02	0.01	0.01	0.01	<0.01	45.7	99.56	2.5181
Pahuntoi	R5996	1.03	0.007	0.05	0.2	0.13	0.06	30.8	21.4	0.03	0.01	0.02	0.01	<0.01	45.8	99.41	2.6181
Pahuntoi	R5997	1.68	0.007	0.08	0.19	0.13	0.06	30.3	20.7	0.02	0.02	0.01	0.01	<0.01	45.4	98.46	2.5663
Pahuntoi	R5998	1.17	0.01	0.13	0.21	0.13	0.06	31.2	20.4	0.02	0.02	0.02	0.01	<0.01	45.4	98.65	2.5301
error	all	2.705	0.06	0.825	0.395		0.22	0.18	0.11	0.13	0.025	0.030				0.35	0.009

Note: Samples are all R-numbers but fossils are F110148 and F123803 in the Condon Collection, University of Oregon. Errors are from 10 replicate analyses of the standard, CANMET SDMS2 (British Columbia granodioritic sand).

Table 2—Trace element composition (ppm) from XRF of Ediacaran rocks from California.

Sample	Ba	Ce	Cr	Cs	Dy	Er	Eu	Ga	Gd	Hf	Ho	La	Lu	Nb	Nd	Pr
R5658	412	51.1	20	0.46	5.34	3.16	1.27	2.9	5.96	8.9	1.09	16.5	0.46	4.3	24.2	5.31
R5659	454	52.2	20	0.45	5.41	3.34	1.28	2.6	6.43	8.1	1.18	17.1	0.46	3.8	24.3	5.41
R5660	449	51.9	20	0.53	5.55	3.21	1.36	3.1	6.52	8.1	1.23	16.3	0.44	3.8	25.9	5.47
R5661	432	58.6	30	0.5	6.04	3.69	1.43	3	7.39	9.7	1.31	19.3	0.51	4.7	28.2	6.2
R5662	420	57.3	30	0.62	5.7	3.31	1.45	3.1	7.24	10.2	1.24	18.8	0.51	4.7	27.6	5.92
F110148	6.3	6	<10	0.03	0.53	0.29	0.07	0.2	0.52	0.3	0.11	2.1	0.04	0.4	2.3	0.54
F123803	153	22.3	10	0.31	1.7	1.16	0.33	1.6	1.67	5.7	0.33	9.4	0.15	5.5	10.5	2.5
R5982	1825	3.5	<10	0.4	0.5	0.27	0.09	1.3	0.47	0.2	0.08	1.7	0.05	0.4	1.9	0.45
R5983	97.5	2.1	<10	0.1	0.15	0.14	0.04	0.3	0.2	0.1	0.04	1	0.01	0.2	0.9	0.25
R5984	259	1.4	<10	0.1	0.14	0.06	0.03	0.3	0.22	<0.1	0.02	0.8	0.01	0.1	0.5	0.16
R5985	178	1.7	<10	0.05	0.17	0.05	0.05	0.4	0.13	<0.1	0.04	1	0.01	0.1	0.8	0.18
R5992	26.4	0.6	<10	0.02	0.03	0.02	0.01	0.3	0.08	<0.1	0.02	0.3	<0.01	0.1	0.3	0.06
R5993	30	0.7	<10	0.03	0.03	0.03	0.01	0.3	0.1	<0.1	0.01	0.4	<0.01	0.1	0.4	0.11
R5994	24.1	0.6	<10	0.04	0.03	0.06	0.01	0.2	0.03	<0.1	0.01	0.4	<0.01	0.1	0.3	0.08
R5995	15.1	0.5	<10	0.04	0.03	0.04	0.01	0.1	0.05	<0.1	0.007	0.3	<0.01	0.1	0.3	0.09
R5996	18.1	0.7	<10	0.04	0.03	0.04	0.01	0.1	0.03	0.1	0.01	0.4	0.01	0.1	0.3	0.1
R5997	23.9	1.9	<10	0.02	0.19	0.13	0.08	0.8	0.12	<0.1	0.01	1.1	0.03	0.3	0.8	0.2
R5998	42.8	1.3	<10	0.05	0.03	0.02	0.01	0.3	0.06	0.1	0.01	0.7	<0.01	0.2	0.6	0.12
error	3.5	0.8	10	0.05	0.05	0.03	0.02	0.1	0.05	0.1	0.01	0.4	0.01	0.1	0.3	0.07

Sample	Rb	Sm	Sn	Sr	Ta	Tb	Th	Tm	U	V	W	Y	Yb	Zr
R5658	31.7	6.51	<1	399	0.4	0.91	5.11	0.43	2.54	18	1	30.2	3.18	367
R5659	31.5	6.36	<1	434	0.4	1.04	4.98	0.44	2.59	20	1	30.9	3.09	349
R5660	33.2	7.14	<1	401	0.3	0.97	5.05	0.48	2.23	18	1	31.2	3.28	342
R5661	32.8	7.92	<1	547	0.5	1.1	6.75	0.45	2.96	21	1	34.3	3.27	388
R5662	31.8	7.15	<1	442	0.4	1.12	5.68	0.51	2.22	21	1	33.9	3.13	431
F110148	1.5	0.59	<1	126	<0.1	0.07	1.03	0.04	0.88	<5	<1	3.1	0.28	13
F123803	21.7	1.86	<1	70.6	0.3	0.29	6.43	0.15	4.2	29	2	8.9	0.99	220
R5982	7.9	0.38	1	218	<0.1	0.06	0.66	0.04	1.41	9	2	3	0.28	7
R5983	0.9	0.3	<1	168	<0.1	0.05	0.34	0.02	0.84	<5	2	1.4	0.15	5
R5984	0.5	0.18	<1	132	<0.1	0.02	0.13	<0.01	0.9	<5	3	0.9	0.04	2
R5985	0.4	0.18	<1	192.5	<0.1	0.03	0.19	0.01	0.87	8	3	1	0.08	2
R5992	0.4	0.06	<1	64.4	<0.1	0.007	0.08	<0.01	0.61	<5	1	0.3	0.03	3
R5993	0.4	0.08	<1	72.5	<0.1	0.01	0.12	0.01	0.66	<5	1	0.5	0.07	2
R5994	0.3	0.05	<1	64.8	<0.1	0.01	0.07	<0.01	0.64	<5	1	0.3	0.03	2
R5995	0.2	0.03	<1	61.3	<0.1	0.01	0.1	<0.01	0.66	<5	2	0.3	0.03	2
R5996	0.4	0.09	<1	66.1	<0.1	0.007	0.12	<0.01	0.65	<5	1	0.4	0.02	2
R5997	1	0.24	<1	59.7	<0.1	0.02	0.32	0.01	0.59	5	1	0.6	0.02	2
R5998	1	0.08	<1	97.3	<0.1	0.01	0.24	<0.01	1.04	5	1	0.5	0.04	3
error	0.2	0.06	1	3.5	0.1	0.01	0.09	0.01	1	5	1	0.3	0.03	2

Note: Samples are all R-numbers but fossils are F110148 and F123803 in the Condon Collection, University of Oregon.

Table 3—Grain-size data from point counting thin sections (500 points) of Ediacaran rocks from California.

Pedotype	Hoz	No.	% grav- el	% sand	% silt	% clay	Textural class	Grain fabric	Plasmic fabric
sandstone	top	R5658	0	26.8	53.6	19.6	silt loam	intertextic	silasepic
sandstone	middle	R5659	0	27.6	53.2	19.2	silt loam	intertextic	silasepic
sandstone	middle	R5660	0	27.8	53.4	18.8	silt loam	intertextic	silasepic
sandstone	middle	R5661	0	27.4	54.4	18.2	silt loam	granular	silasepic
sandstone	bottom	R5662	0	25.4	57.0	17.6	silt loam	granular	silasepic
Nataanga	above	R5981	0	24.2	50.8	25.0	silt loam	intertextic	silasepic
Nataanga	A	R5982	0	13.8	50.6	35.6	silty clay loam	agglomeroplastic	insepic
Nataanga	A	R5983	0	27.4	42.6	30.0	clay loam	agglomeroplastic	insepic
Nataanga	C	R5984	0	30.2	46.2	23.6	loam	agglomeroplastic	insepic
Nataanga	C	R5985	0	34.0	55.6	10.4	silt loam	intertextic	calciasepic
Paka	above	R5986	37.4	14.0	38.6	10.0	silt loam	granular	calciasepic
Paka	A	R5987	4.8	34.4	41.2	19.6	loam	agglomeroplastic	insepic
Paka	Bw	R5988	3.2	21.4	53.6	21.8	silt loam	agglomeroplastic	insepic
Paka	R	R5989	32.4	22.2	38.0	7.4	silt loam	agglomeroplastic	calciasepic
Paka	R	R5990	18.2	31.0	42.6	8.2	silt loam	agglomeroplastic	calciasepic
Pahuntoi	above	R5991	2.6	35.0	43.4	19.0	loam	agglomeroplastic	calciasepic
Pahuntoi	A	R5992	1.6	34.2	38.8	25.4	loam	agglomeroplastic	insepic
Pahuntoi	A	R5993	2.2	36.8	38.6	22.4	loam	agglomeroplastic	insepic
Pahuntoi	Bw	R5994	2.6	37.4	34.2	25.8	loam	agglomeroplastic	calciasepic
Pahuntoi	Bw	R5995	1.4	42.8	36.4	20.4	loam	agglomeroplastic	calciasepic
Pahuntoi	Bw	R5996	7.6	34.2	38.0	20.2	loam	agglomeroplastic	calciasepic
Pahuntoi	C	R5997	0.2	23.8	62.2	13.8	silt loam	agglomeroplastic	calciasepic
Pahuntoi	C	R5998	1.2	45.6	42.2	11.0	loam	agglomeroplastic	calciasepic

et al., 2018), and hence the new names in this article are effectively published from the electronic edition alone. In addition, new names contained in this work have been submitted to MycoBank from where they will be made available to the Global Names Index. The unique Mycobank number can be resolved and the associated information viewed through any standard web browser by appending the Mycobank numbers to the prefix <https://www.mycobank.org/MB/>. *Ganarake scalaris* new genus and species described here are registered as #843123 and #843137, respectively. All figured specimens are archived in the Condon Collection of the Museum of Natural and Cultural History of the University of Oregon: rock specimen numbers are prefixed **R** and fossil specimen numbers are prefixed **F**.

WAS NOONDAY FORMATION A MARINE WHITING OR TERRESTRIAL LOESS?

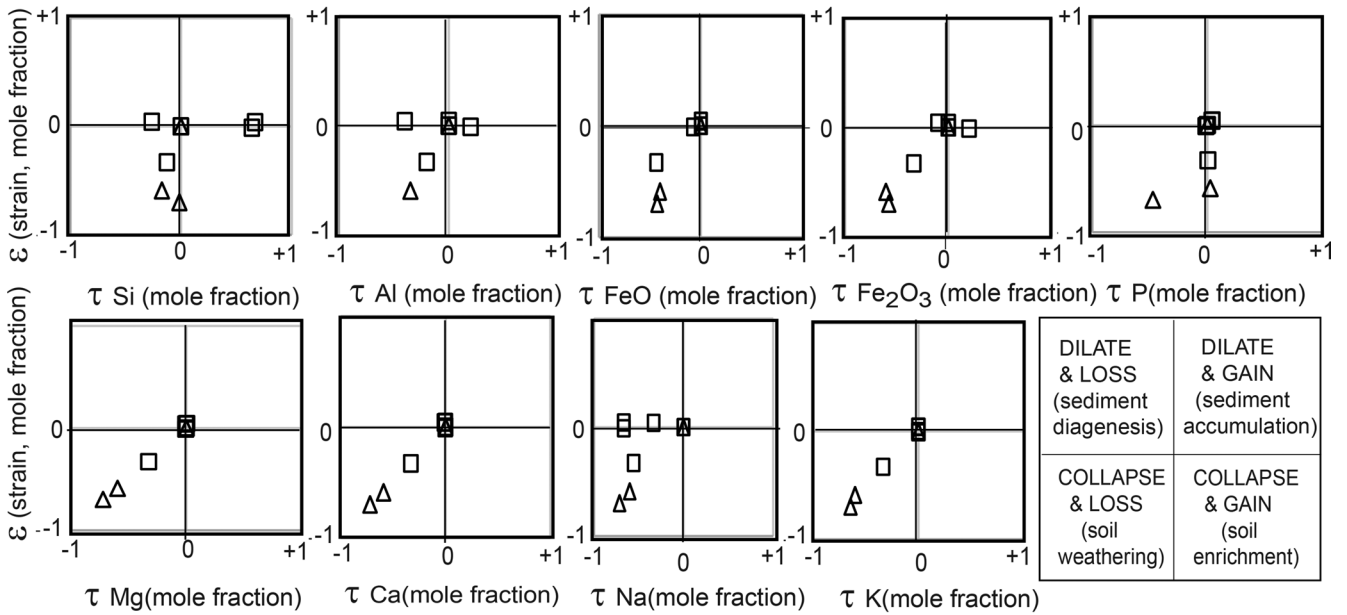
“Cap carbonates” like the Noonday Formation are known globally above Neoproterozoic tillites and envisaged as an abrupt alkalization of the world ocean following greenhouse termination and sea level rise after global glaciation of Snowball Earth (Hoffman & Schrag, 2002; Hoffman, 2011). Holocene marine limestones or dolostones are unknown above Pleistocene tills so this explanation is without clear modern analogs. Modern alkalization events are called whittings, and are clouds of acicular aragonite and calcareous plankton formed in lakes and oceans by plankton-induced changes toward markedly more alkaline pH (Thompson *et al.*, 1997; Sondi & Juračić, 2010; Long *et al.*, 2017).

An alternative explanation for carbonates above tillites advanced for the comparable earliest Ediacaran Nucaaleena

Table 4—Mineral content from point counting thin sections (500 points) of Ediacaran rocks from California.

Pedotype	Hoz	No.	% clay	% do- lomite needles	% do- omite spar	% do- lomite rhombs	% rock	% feld- spar	% mica	% quartz	% opaque
sandstone	top	R5658	21.8	0	0	1.0	2.4	31.6	5.6	35.2	2.4
sandstone	middle	R5659	22.4	0	0	0	1.8	34.8	8.0	29.6	3.4
sandstone	middle	R5660	23.8	0	0	0	4.6	34.4	3.4	29.8	4.0
sandstone	middle	R5661	25.4	0	0	0	3.8	32.0	3.6	32.0	3.2
sandstone	bottom	R5662	20.0	0	0	0	4.6	33.6	5.4	33.2	3.2
Nataanga	above	R5981	25.6	0	0	45.0	1.0	15.4	0.6	10.2	2.2
Nataanga	A	R5982	37.2	0	0	16.8	4.4	22.2	0	15.8	3.6
Nataanga	A	R5983	32.8	0	0	45.6	5.8	7.8	0.6	6.4	1.0
Nataanga	C	R5984	25.4	0	0	42.0	3.6	12.4	0.4	9.6	3.4
Nataanga	C	R5985	11.2	0	0	50.4	6.6	17.0	0.2	13.0	1.6
Paka	above	R5986	7.0	0	0	42.6	3.6	23.8	4.4	17.0	1.6
Paka	A	R5987	22.6	12.0	8.4	23.0	2.8	16.0	0.2	11.2	3.8
Paka	Bw	R5988	23.6	1.4	3.2	48.8	1.0	10.8	0.2	9.6	1.4
Paka	R	R5989	7.6	16.8	37.6	31.4	1.6	2.0	0.6	2.2	0.2
Paka	R	R5990	7.2	13.0	16.2	49.0	1.2	4.6	3.8	4.4	0.6
Pahuntoi	above	R5991	21.6	0	3.2	55.0	1.2	8.0	1.6	7.2	2.2
Pahuntoi	A	R5992	29.2	2.2	7.8	42.2	1.8	7.4	1.6	5.6	2.2
Pahuntoi	A	R5993	22.2	2.8	3.0	50.8	0.4	8.6	1.6	6.6	4.0
Pahuntoi	Bw	R5994	27.2	4.0	2.8	42.8	2.4	9.2	3.2	6.0	2.4
Pahuntoi	Bw	R5995	21.4	5.2	7.6	45.4	1.2	7.0	4.6	5.8	1.8
Pahuntoi	Bw	R5996	22.0	19.6	6.6	44.0	0.2	2.8	1.2	2.2	1.4
Pahuntoi	C	R5997	13.6	0.6	0.4	64.2	3.4	3.4	8.4	2.4	3.6
Pahuntoi	C	R5998	14.8	0.4	3.6	49.4	2.4	8.4	8.4	9.2	3.4

A. mass transfer with strain



B. mass transfer with depth

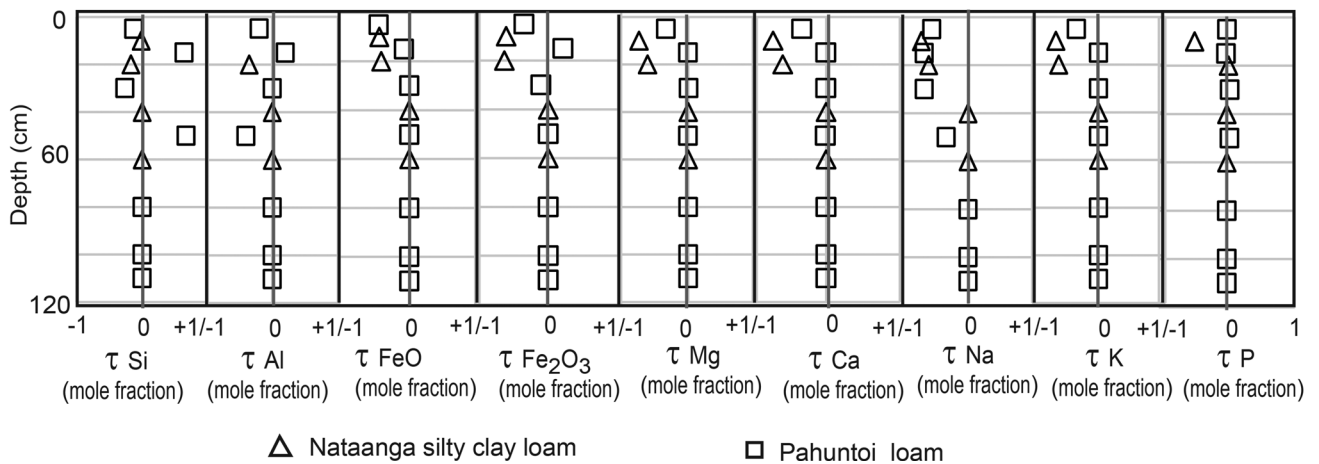


Fig. 6—Tau analysis of Noonday Formation beds with strain (A) and with depth (B). Zn was used as the stable constituent. These arrays are typical for weakly developed soils.

Formation of South Australia (Retallack, 2011), is that they are calcareous loess with paleosols like Quaternary Peoria Loess above Illinoian till (Bettis *et al.*, 2003; Wang *et al.*, 2006), or the Quaternary Chinese Loess Plateau onlapping montane glacial moraines (Derbyshire, 2001; Sun, 2002; Sun *et al.*, 2010). Paleosols in loess are most decisively recognized from fossil root traces (Retallack, 1991), but Ediacaran rocks are too old for vascular land plants (Retallack, 2015a, b), so other features must be used, such as within-bed petrographic and chemical composition, granulometry, crystal fans, carbonate shrubs, YREE content, stable isotopic covariation, and ravinement surfaces. The following paragraphs explore each of these paleosol criteria for the Noonday Formation

as evidence for choosing between a marine whitening versus post-glacial loess-paleosol interpretation.

Within-bed petrographic and chemical composition

The Noonday Formation platform facies is mainly dolomite, including silt-sized subrounded grains (Fig. 4E), with rock fragments, feldspar and quartz (Fig. 4B). Dolomite has replaced sparry calcite in tubestone cores (Fig. 4A, 4D), spherulites of needle-fiber calcite (Fig. 4C), and skeletal bipyramidal acicular crystals after whewellite (Fig. 4F). An important discovery of this study is that the tubestones are not continuous for more than a meter vertically within individual beds (fig. 3): they go to the top of the bed where they may

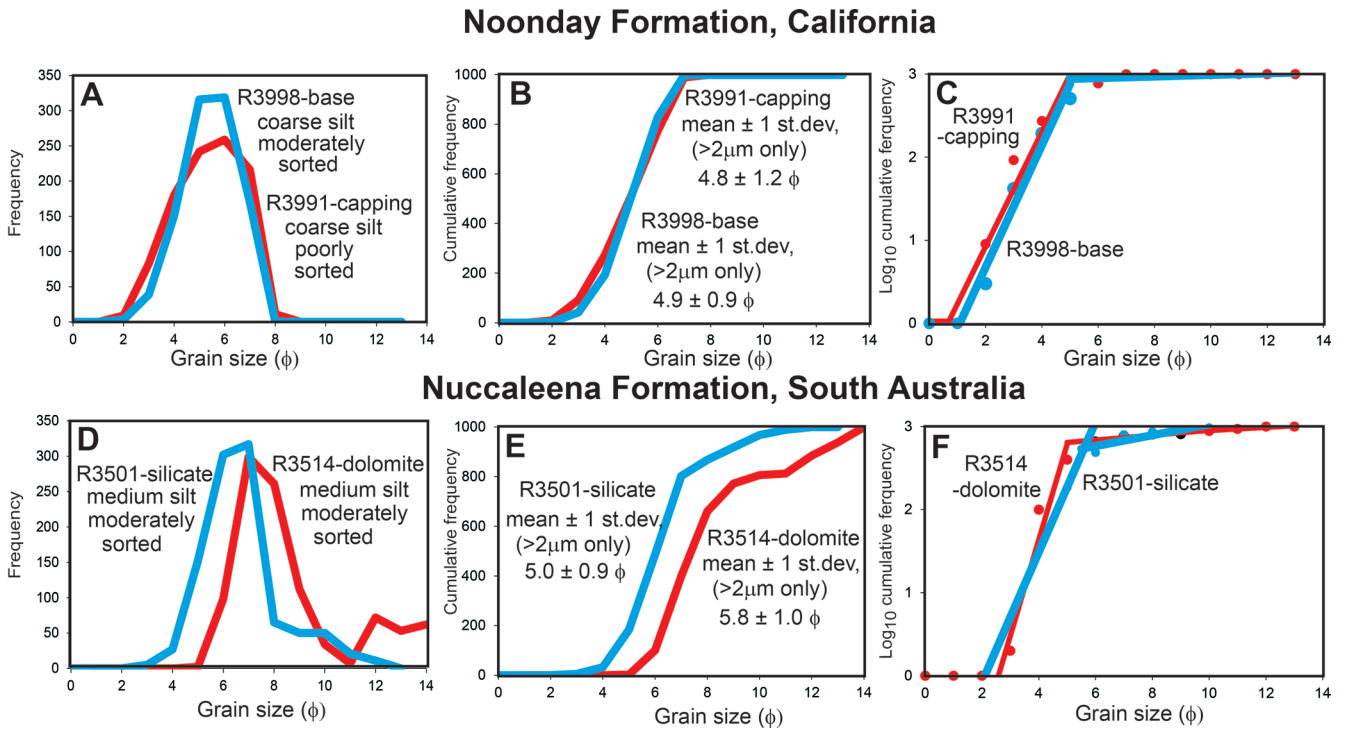


Fig. 7—Granulometry of Noonday Formation (A–C), compared with early Ediacaran Nuccaleena Formation of South Australia (D–F). Separate plots are frequency (A, D), cumulative frequency (B, E) and semilog cumulative frequency (C, F), all from measuring long axes of 1000 grains in thin section (D–F from Retallack, 2011).

deviate from vertical, but remain vertical like a plumb-bob to near the base of the bed with clear bedding planes (Fig. 5), even in outcrops with low-angle primary dips in Galena Canyon (Fig. 2B).

Point counting of thin sections of individual beds shows clay enrichment toward the top of beds, usually at the expense of dolomite and rock fragments (Fig. 5). In addition to clay there also are significant amounts (8–50 volume percent) of silicate minerals, mainly quartz and feldspar. Carbonate is depleted toward the surface of the beds and this is reflected in molar ratios of $\text{CaO} + \text{MgO}/\text{Al}_2\text{O}_3$. One bed shows soda enrichment, but total cationic bases were depleted in both analyzed beds. Leaching is modest in the surface of one bed from Ba/Sr molar ratios, but other samples in both beds show only modest leaching. Chemical reduction (gleization) from $\text{FeO}/\text{Fe}_2\text{O}_3$ ratios is modest in all profiles, and two of the three profiles are red with hematite (Fig. 5).

A more sophisticated method to disentangle soil formation from sedimentation is tau analysis (Brimhall *et al.*, 1992). Tau analysis isolates two separate aspects of weathering: mole fraction mass transport ($\tau_{j,w}$) of a mobile element and mole fraction strain ($\epsilon_{i,w}$) of an immobile element, using the following formula including bulk density (ρ in $\text{g}\cdot\text{cm}^{-3}$) and oxide assay (C in weight %) for successive samples (subscripts i,j) of weathered material (subscript w) and parent material (subscript p).

$$\epsilon_{i,w} = \left[\frac{\rho_p C_{j,p}}{\rho_w C_{j,w}} \right] - 1 \quad \text{— equation 1}$$

$$\tau_{j,w} = \left[\frac{\rho_w C_{j,w}}{\rho_p C_{j,p}} \right] [\epsilon_{i,w} + 1] - 1 \quad \text{— equation 2}$$

Soils and paleosols lose mass with weathering and so have negative strain ($\epsilon_{i,w} < 0$), and also lose nutrient cations and silica, so have negative mass transfer ($\tau_{j,w} < 0$). In contrast, sediment accumulation and diagenetic alteration adds elements and mass so has positive strain and mass transfer (Retallack *et al.*, 2021b). Tau analysis has been widely used for Precambrian paleosols (Retallack & Mindszenty, 1994; Driese *et al.*, 2011), as well as Cenozoic paleosols (Bestland *et al.*, 1996; Sheldon & Tabor, 2009), and modern soils (Chadwick *et al.*, 1990; Hayes *et al.*, 2019). In this case, Zn was used as a stable constituent, because Ti was beyond detection in some samples. Sample R5996 was used as parent for the Pahuntoi bed, and R5984 for the Nataanga bed. All samples are within the soil rather than sediment field, and the degree of soil development in the Nataanga bed is greater than for the Pahuntoi bed (Fig. 3). In both beds, depth and intensity of chemical weathering is shallow (Fig. 6), even compared with other Ediacaran paleosols (Retallack, 2011, 2013, 2021).

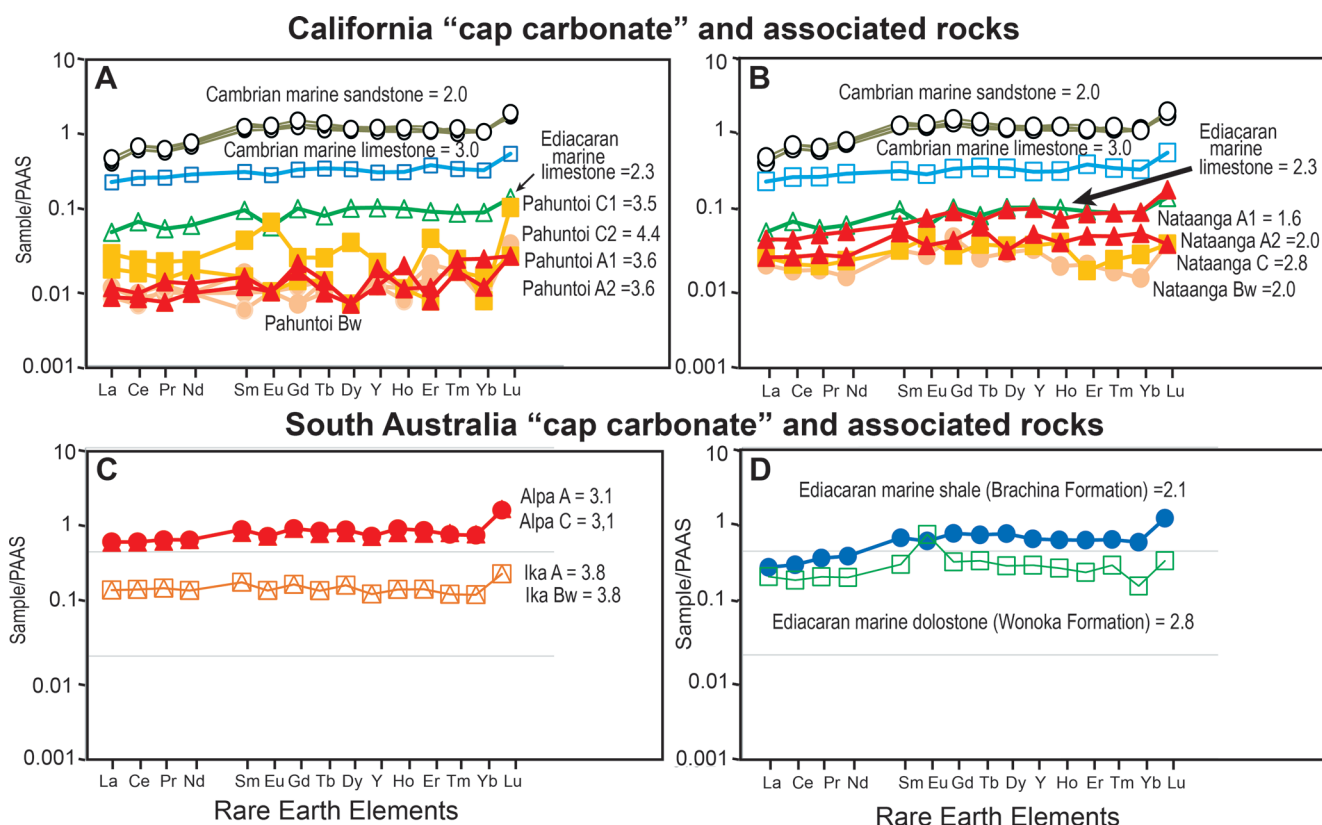


Fig. 8—Rare Earth Element and yttrium analyses. (A–B) named Noonday Formation beds, compared with marine limestone of the Johnnie Formation near Noonday Mine, and of Cambrian marine limestone and sandstone of the Wood Canyon Formation in Emigrant Pass east of Tecopa, California; (C–D) comparable analyses of the Nuccaleena Formation and associated marine beds in South Australia.

Variable and sometimes high siliciclastic content are additional evidence against marine precipitation of these beds. Marine whittings are uniform micritic mud of aragonite laths, and commonly contain planktonic microfossils (Thompson *et al.*, 1997; Sondi & Juračić 2010; Long *et al.*, 2017). Acanthomorphic acritarchs regarded as planktonic microfossils are common in Cryogenian and Ediacaran rocks (McFadden *et al.*, 2009; MacDonald *et al.*, 2010; Butterfield, 2015), but were not seen in thin sections or palynological preparations made for this study of the Noonday Formation, as further evidence against its aquatic origin. Clay enrichment of bed tops does not appear to be part of graded beds such as turbidites deposited in a water column, for several reasons (Fig. 5): scarce clay, red colors, dominance of silt and sand, and lack of coordinated surface enrichment in alumina, lime and magnesia found in genuine turbidites (Komar, 1985; Korsch *et al.*, 1993).

Observed petrographic and chemical trends are like those of paleosols, rather than marine beds, showing characteristic surface truncation and gradational alteration down from that surface. Modest surficial clay enrichment and carbonate depletion is compatible with hydrolytic weathering of silicate minerals and dissolution of carbonate as in soils and

paleosols of calcareous loess with dustings of quartz and feldspar (Bettis *et al.*, 2003; Retallack, 2011; Sun *et al.*, 2010). Within soil classifications, the Pahuntoi loam would have been a Psamment (Soil Survey Staff, 2014), Regosol (Food & Agriculture Organization, 1974), and Calcareous Sand (Stace *et al.*, 1968). Similarly, the Nataanga silty clay loam was an Ochrept (Soil Survey Staff, 2014), Cambisol (Food & Agriculture Organization, 1974), and Desert Loam (Stace *et al.*, 1968), respectively, and the Paka loam was an Orthent (Soil Survey Staff, 2014), Lithosol (Food & Agriculture Organization, 1974), and Terra Rossa (Stace *et al.*, 1968), respectively. These comparable modern soils are all well drained profiles that could not form in marine settings.

Granulometry

A surprise from point counting Noonday Formation beds was the high proportion of angular silt grains, between 34.2 and 66.2 volume %. These beds were unusually silt-rich, and lacked fine lamination except at the bottom of the massive bed, or in overlying material. One bed had fragments of angular dolostone in red micritic matrix filling narrow and deep crevices within the underlying rock (Fig. 5). Long axes

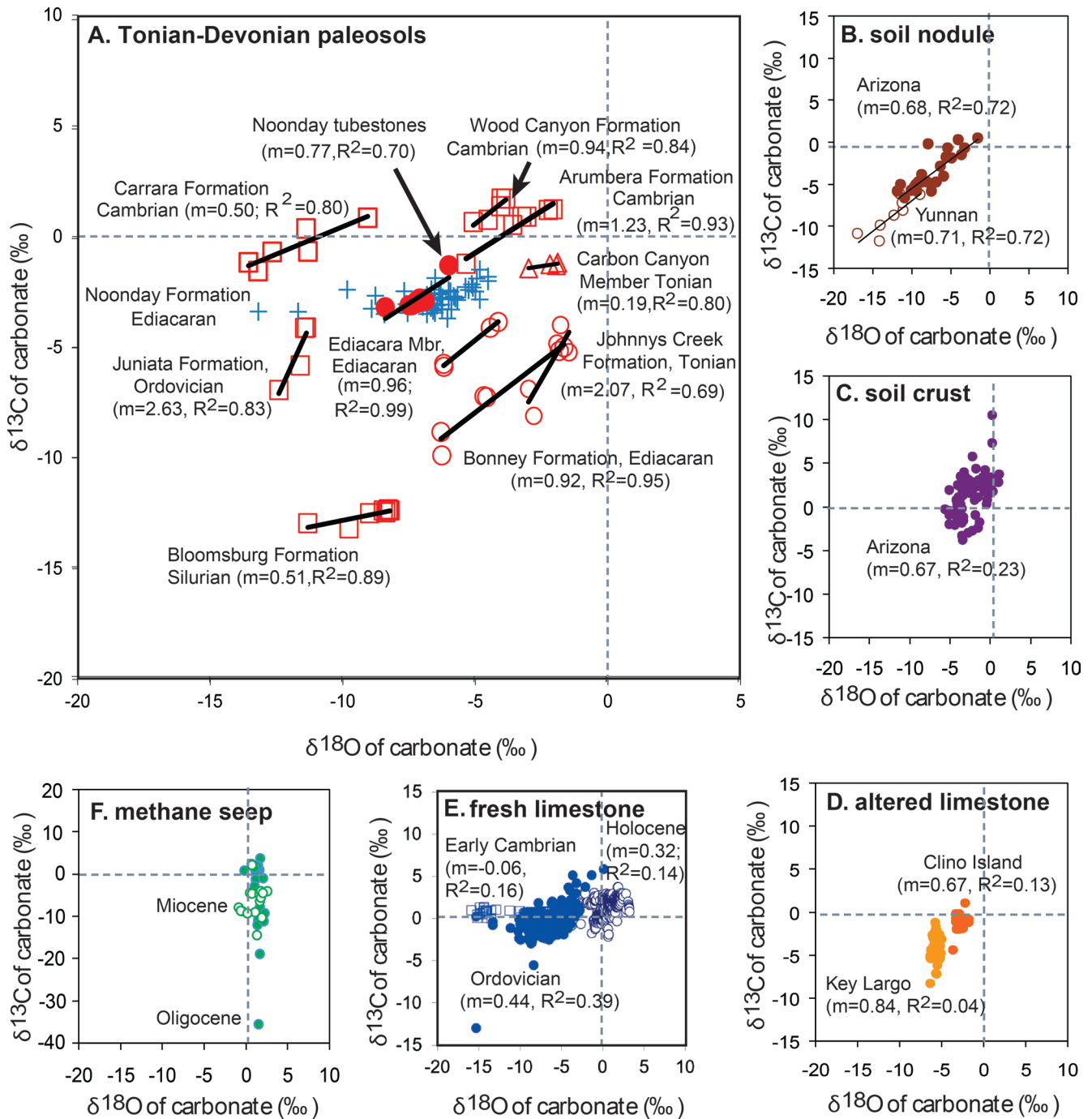


Fig. 9—Stable isotopic covariation of Noonday Formation tubestones. (A) lack of correlation in marine-derived clasts of the Noonday Formation, compared with correlated pedogenic carbonate of Noonday Formation pedogenic carbonate (tubestones herein), Ediacaran paleosols of South Australia (Retallack, 2013, 2016, 2021), Cambrian Arumbera Formation at Ross River (Retallack & Broz, 2020), Ordovician paleosols of Pennsylvania (Retallack, 2015a), and Silurian paleosols of Pennsylvania (Retallack, 2015b); (B) soil nodules above Woodhouse lava flow, near Flagstaff, Arizona (Knauth *et al.*, 2003) and in Yuanmou Basin, Yunnan, China (Huang *et al.*, 2005); (C) soil crusts on basalt Sentinel Volcanic Field, Arizona (Knauth *et al.*, 2003); (D) Quaternary marine limestone altered diagenetically by meteoric water, Key Largo, Florida (Lohmann, 1988) and Cliño Island, Bahamas (Melim *et al.*, 2004); (E) Holocene (open circles) and Ordovician (open squares) unweathered marine limestones (Veizer *et al.*, 1999) and Early Cambrian (closed circles), Ajax Limestone, South Australia (Surge *et al.*, 1997); (F) marine methane cold seep carbonate, Miocene, Santa Cruz Formation, Santa Cruz, California (Aiello *et al.*, 2001) and Oligocene, Porter, Washington (Peckmann *et al.*, 2002). Slope of linear regression (m) and coefficients of determination (r²) show that carbon and oxygen isotopic composition is significantly correlated in soils and paleosols, but not in other settings.

A. Chinese loess plateau and sand deserts

B. Chinese loess sequence Lingtai

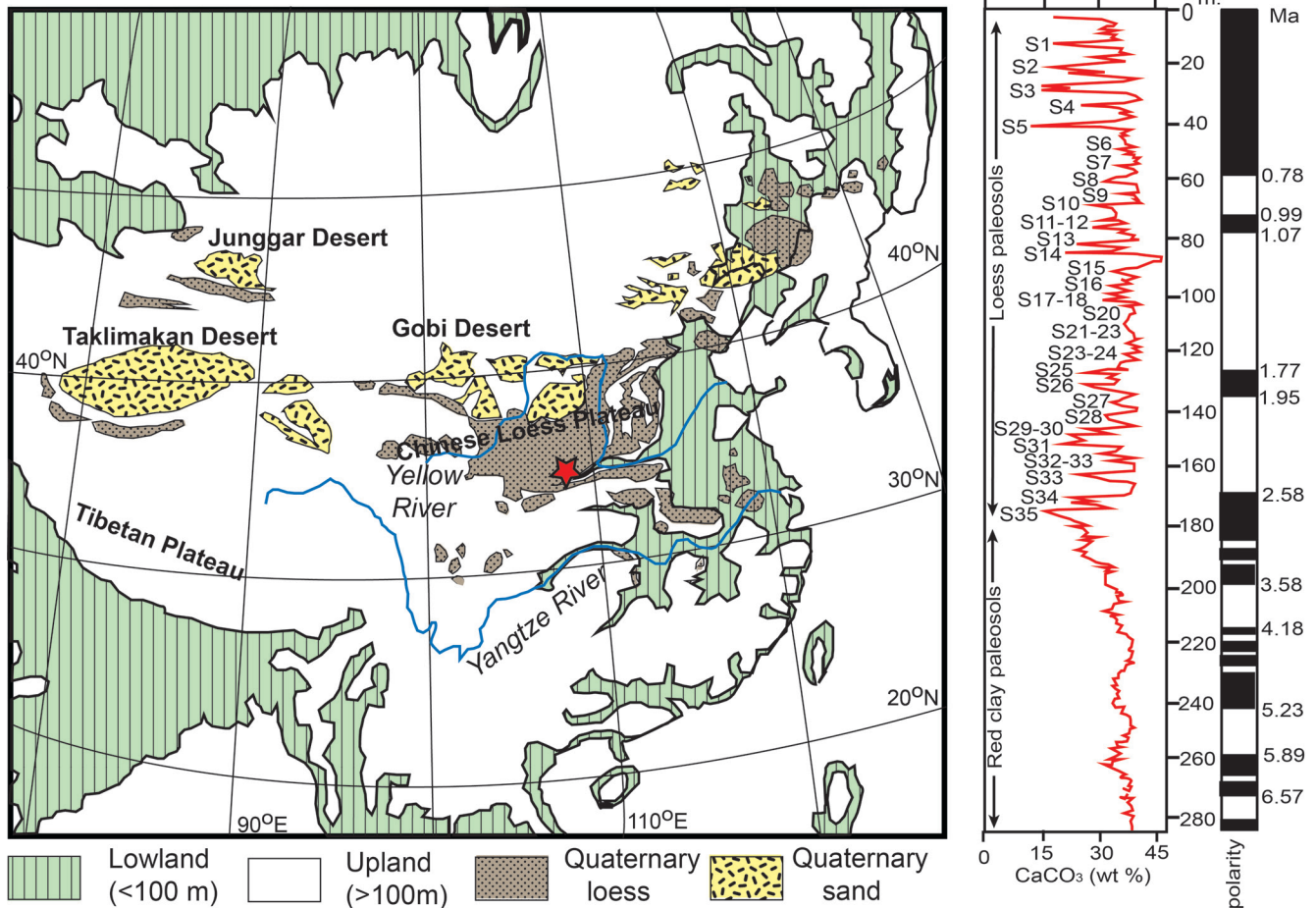


Fig. 10—Chinese Loess Plateau as a modern analog for Noonday Formation. (A) geographic setting (data from Sun, 2002); (B) paleosol sequence (data from Sun *et al.*, 2010).

of 1000 grains were measured from two of the thin sections and had a mean grain size of 4.9Φ ($44 \mu\text{m}$), which is coarse silt, and moderately sorted (standard deviation $\pm 0.9 \Phi$ or $\pm 37 \mu\text{m}$), similar to another early Ediacaran “cap carbonate” of the Nuccaleena Formation (Fig. 7).

This size distribution is unlike that of marine whittings which are mostly grains finer than $5 \mu\text{m}$ (7.6Φ), which is fine silt (Thompson *et al.*, 1997), although the coarse tail of whitening size-distributions can have grains $32\text{--}63 \mu\text{m}$ ($5.0\text{--}4.0 \Phi$) in a distribution much wider than observed in the Noonday Formation (Sondi & Juračić, 2010). Whittings also have acicular to lath-like crystals only and little quartz or feldspar (Sondi & Juračić, 2010), unlike the mostly equant crystals of Noonday Formation (Fig. 4B).

Silt-rich beds of the Noonday Formation may have been loess, deposited on land by wind. Much eolian silt may have fallen into the sea before landscapes were stabilized by plants, but the Noonday examples are grain supported (Fig. 4B), not embedded in clay and carbonate as observed in Cambrian

marine siltstones (Dalrymple *et al.*, 1985). Silt-rich beds of the Noonday Formation are similar in grain size, angularity, and texture (Fig. 5) to Quaternary Peoria Silt ($5.5\text{--}4.5 \pm 0.4\text{--}0.9 \Phi$, or $51\text{--}21 \mu\text{m}$ (Swineford & Frye, 1951; Pye & Sherwin, 1999), which has 31–42% limestone and dolomite clasts (Fisk, 1951; Grimley *et al.*, 1998)). Chinese loess of the Central Loess Plateau is similar (modal grain sizes $5.0\text{--}6.6 \Phi$, or $32\text{--}10 \mu\text{m}$ (Nugteren *et al.*, 2004; Sun *et al.*, 2004)). Both Chinese and Peoria loess with paleosols pass laterally into eolian sand paleodunes with coarser and less well sorted grain size (Bettis *et al.*, 2003; Long *et al.*, 2012), like those of Galena Canyon (Fig. 2B). Compositional differences in Pleistocene Peoria Loess reflect proximity to freshly deglaciated Paleozoic limestones and dolostones in Illinois and Wisconsin, but for the Noonday Formation the source of carbonate silt-size clasts would have been glaciated Mesoproterozoic Beck Spring and Crystal Spring marine dolostones with stromatolites (Wright *et al.*, 1976; Corsetti & Kaufman, 2003). Other similar eolian loess deposits are the basal Ediacaran Nuccaleena Formation

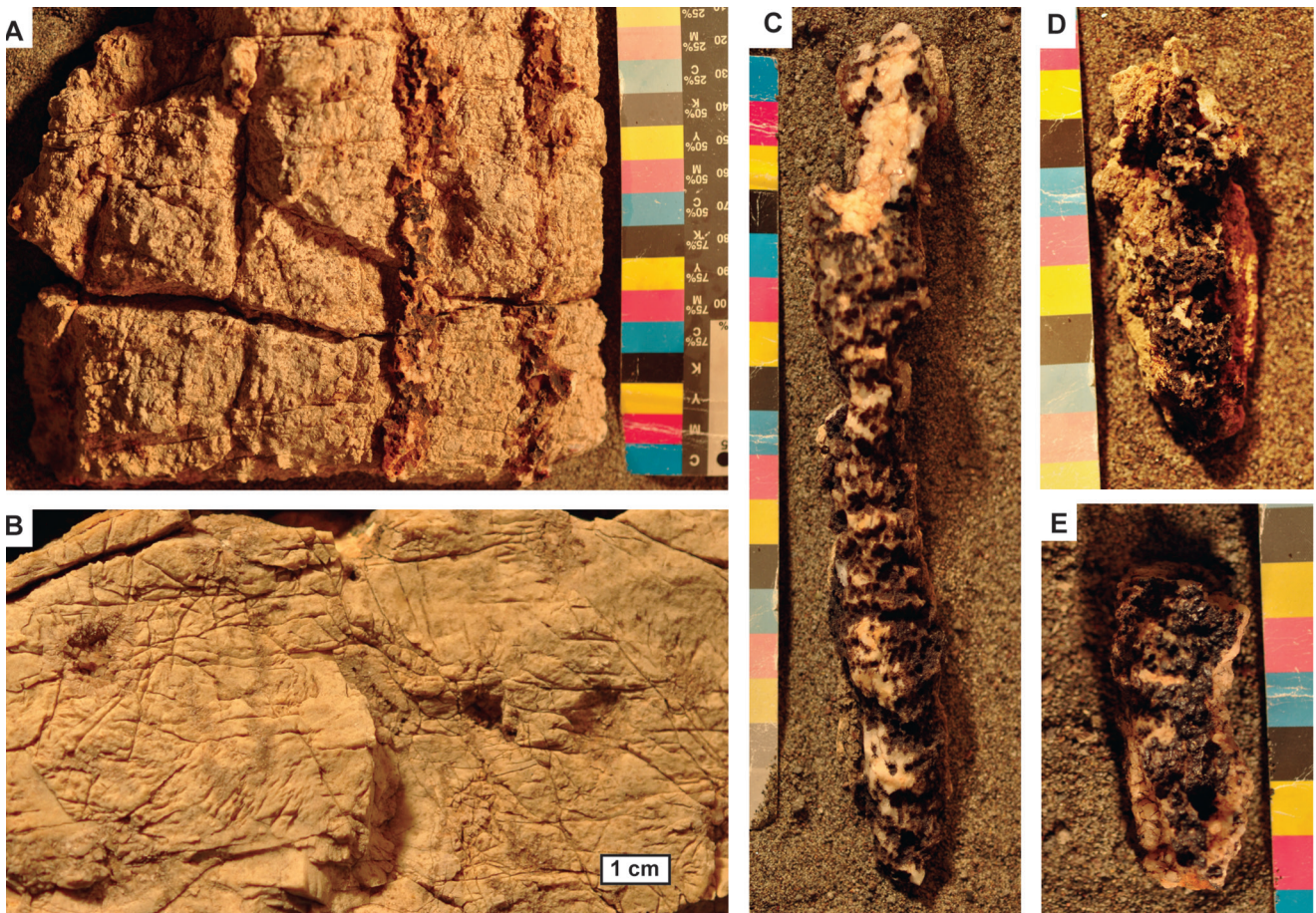


Fig. 11—*Ganarake scalaris* gen et sp. nov. macromorphology. (A–B) specimens in matrix; (C–E) weathered out silicified specimens from Galena Canyon. Horizontal ridges in panels 3–4 are edges of invaginated cups. Specimen numbers in the Condon Collection of the Museum of Natural and Cultural History, University of Oregon are F116110A (A), F11662B (B), F116111A (C), F116111F (D) and F116111E (E). The color scales are in cm.

of South Australia (Retallack, 2011), upper Moonlight Valley Tillite and lower Ranford Formation of Western Australia (Retallack, 2021), Arumbera Formation of central Australia (Retallack & Broz, 2020), Late Ediacaran Ediacara Member of South Australia (Retallack, 2013; McMahon *et al.*, 2020), and Late Cambrian Mount Simon Sandstone of Illinois (Reesink *et al.*, 2020).

Crystal fans, sheet cracks, and carbonate shrubs

Neoproterozoic “cap carbonates” are distinguished by a variety of structures that have been considered unique to them (Hoffman, 2011), and also observed in the Noonday Formation. Crystal fans are spherulites (Fig. 4C, 4F) or partial splays (Fig. 4D) of acicular carbonate crystals. Some of these spherulites are isolated, but they also form dark dendritic growths (Fig. 4C), which have been called “carbonate shrubs” (Fraiser & Corsetti, 2003). Sheet cracks are subhorizontal openings with cavity-lining sparry crystals (Fig. 4C–D).

The sheet cracks have been interpreted as “areas of pore–fluid overpressures in the presence of an alkalinity pump (anaerobic respiration?), possibly related to ice–sheet meltdown and resultant regional sea–level fall” (Hoffman, 2011), and also as “doming, and brecciation of beds by buoyant deformation from methane gas or displacive growth of secondary hydrate” in a marine methane seep (Kennedy *et al.*, 2001). Carbonate shrubs also have been attributed to microbial growth (Cloud *et al.*, 1974), but are non–analog in the sense that microbially–induced carbonate shrubs do not form today under conditions of calcite supersaturation like that proposed for post Cryogenian oceans (Fraiser & Corsetti, 2003). Oligocene and Miocene submarine methane seeps lack bedding–parallel sheet cracks with sparry calcite fill, but do include large (0.5–2 m diameter) vertical pipes unlike Noonday tubestones (Aiello *et al.*, 2001; Peckmann *et al.*, 2002).

An alternative proposal for sheet cracks in Neoproterozoic cap carbonates of China is as small subhorizontal caves,

including stalactites, of paleokarst exposure, which also fossilized terrestrial fungi (Gan *et al.*, 2021). Fungal origin may also explain needle fiber spherulites and shrubs (Fig. 4C), because needle fiber calcite is formed by fungi in calcareous soils and karst (Verrecchia & Verrecchia 1994; Bajnóczy & Kovács–Kis, 2006). Distinctive acicular bipyramidal skeletal grains with quadrangular cross sections (Fig. 4F) are identical to oxalate crystals of weddellite ($\text{CaC}_2\text{O}_4 \cdot 2\text{H}_2\text{O}$), whewellite ($\text{CaC}_2\text{O}_4 \cdot \text{H}_2\text{O}$), and glushinskite ($\text{MgC}_2\text{O}_4 \cdot 2\text{H}_2\text{O}$) produced by fungi, lichens, and plants (Wilson *et al.*, 1980; Hartl *et al.*, 2007; Sturm *et al.*, 2015). Other non-marine indicators of other Ediacaran “cap carbonates” include thufur mounds, linear dunes and climbing–translatent stratification (Retallack, 2011).

YREE

Chemical Composition

Because each local area may have unique europium, cerium, or other anomalies, and different overall YREE (yttrium and rare earth element) concentrations, that are carried forward from source to sink (Bau, 1996), this study uses YREE arrays to distinguish marine and non-marine rocks by comparing samples of similar provenance from California (Fig. 8A–B) and South Australia (Fig. 8C–D). Soils and granites are enriched in light YREE (LYREE), with atomic numbers 57–62, rather than heavy YREE (HYREE), with atomic numbers 63–71, so that the ratio of light to heavy is 3–22 (Minařík *et al.*, 1998; Aubert *et al.*, 2001). In fluvial systems these arrays with negative slope are homogenized to flatter arrays closer to the ratio of 3 (Munemoto *et al.*, 2020). In deep marine clays, the YREE array has a positive slope, and LYREE/HYREE less than 3 (Yasukawa *et al.*, 2015). Hydrothermal alteration of black smokers on the deep-sea floor creates anomalous concentrations of europium (Hongo & Nozaki, 2001). Similar YREE arrays have been found in Archean (3 Ga) rocks despite metamorphism high in the greenschist facies and near total cementation and replacement by silica, which substantially reduced overall YREE concentrations (Bolhar & van Kranendonk, 2007; Sugahara *et al.*, 2010).

For California, three analyzed marine beds all had LYREE/HYREE less than 3: a Cambrian sandstone bed with *Bergaueria* trace fossils in the Wood Canyon Formation, limestone from the Early Cambrian Carrara Formation, and limestone from the Ediacaran Deep Springs Formation (Fig. 8A–B). The five Cambrian sandstone analyses are identical for a bed only 20 cm thick, but the Pahuntoi and Nataanga beds show big differences in arrays spaced only a few centimeters apart (Figs 5, 8A–B). LYREE/HYREE ratios are non-marine (> 3) for the Pahuntoi bed, and marine-influenced (< 3) for the Nataanga bed. Similar ratios and within bed differentiation are also seen in previously studied paleosols (Retallack, 2011)

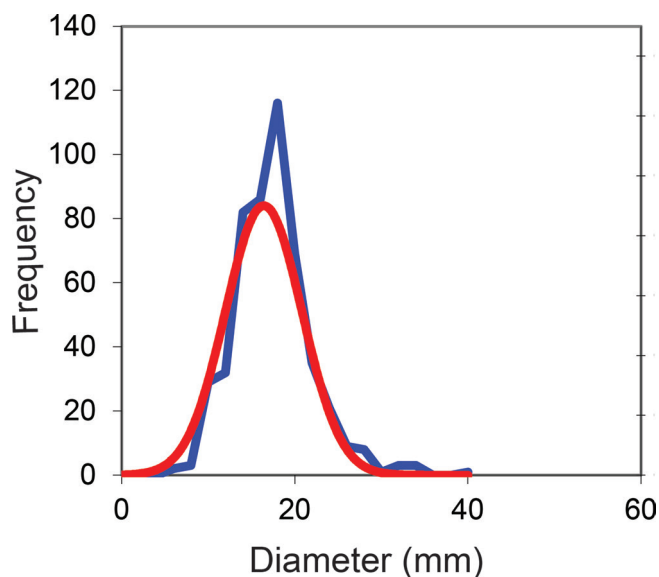


Fig. 12—*Ganarake scalaris* diameter distribution of 500 specimens in Galena Canyon. The blue histogram is raw data, and the normal curve in red was computed from the same mean and standard deviation.

from the earliest Ediacaran Nuccaleena Formation of South Australia (Fig. 8C–D). PAAS-normalized YREE from the Ediacaran Sete Lagoas cap carbonate of Brazil (Caxito *et al.*, 2018) and the Doushantou Formation of China (Huang *et al.*, 2009) are different, showing unusual peaked arrays with heaviest and lightest YREE both depleted, perhaps due to meteoric weathering alternating with deposition of marine carbonate (Gan *et al.*, 2021). There is no evidence of hydrothermal or volcanic alteration of any of the analyzed beds from europium or other anomalies (Sugahara *et al.*, 2010). The Nataanga bed is from the upslope fill of a ravinement surface with 200 m of relief within the Noonday Formation Radcliff Member basinal facies (Creveling *et al.*, 2016), and may have been influenced by marine transgression (Creveling & Mitrovica, 2014). The Pahuntoi bed of the platform facies however was entirely non-marine.

Stable isotopic covariation

Dolomitic tubestones of the Noonday Formation with acicular crystals in spherulites and carbonate shrubs (Fig. 4C) analyzed for stable isotopic composition (Corsetti & Kaufman, 2003) show strong covariance of $\delta^{13}\text{C}$ and $\delta^{18}\text{O}$ (Fig. 9A). However, dolomitic silt of the Noonday Formation (symbol + in Fig. 9A) in the same area shows no such correlation.

Cross-plots of $\delta^{13}\text{C}$ and $\delta^{18}\text{O}$ in marine carbonate have long been used to screen for diagenetic alteration, including soil formation and karst weathering (Retallack, 2016). Unaltered marine limestones and sea-shells (Fig. 9E) show no hint of correlation (Surge *et al.*, 1997; Veizer *et al.*, 1999), and this

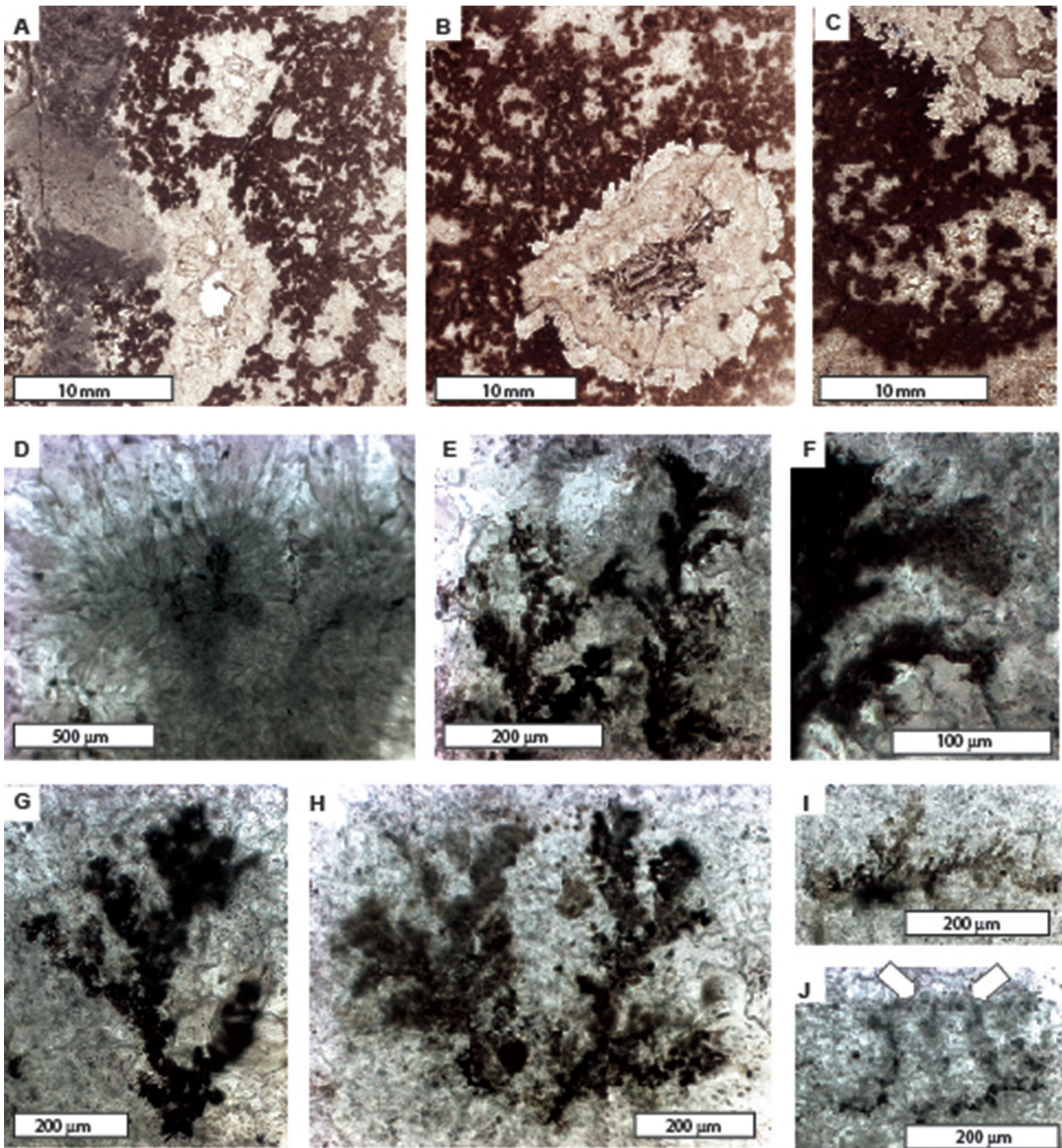


Fig. 13—*Ganarake scalaris* gen et sp. nov. petrographic observations. (A–B) sparry dolomite fill of tubestone and flanking carbonate shrubs; (C) carbonate shrub flank of tubestone; (D) detail of needle fiber calcite of carbonate shrub; (E–I) carbonaceous thalli; (J) fused hyphae (at arrows) forming ladder structure. Specimen numbers in the Condon Collection of the Museum of Natural and Cultural History, University of Oregon are F116110A (A, E–J), F116110C (B–D).

is true for bulk Noonday Formation derived from erosion of older Proterozoic dolostones (Fig. 9A). The most profoundly altered carbonate is pedogenic and fungal carbonate, which is

an early diagenetic precipitation between deposition and burial of alluvial sediment (Retallack, 1991, 2005). Significant ($P > 0.05$) covariance is clear in Holocene soils (Fig. 9B) in China

(Huang *et al.*, 2005) and Arizona (Knauth *et al.*, 2003), and in the Pahuntoi bed and other Cambrian and Neoproterozoic paleosols (Loyd *et al.*, 2012; Retallack *et al.*, 2014, 2021a; Retallack, 2021). Less significant correlations (Fig. 9C–D) are formed in soil carbonate crusts (Knauth *et al.*, 2003), and marine limestone altered by deep circulation of meteoric water (Lohmann, 1988; Melim *et al.*, 2004). Lake carbonates with covariant stable isotopes may also be a case of soil alteration, because covariance is only found in seasonally dry lakes, not perennial open system lakes (Talbot, 1990). Near constant $\delta^{18}\text{O}$ but highly varied $\delta^{13}\text{C}$ (Fig. 9F) is formed by microbial methanogenesis in carbonate of marine methane seeps (Aiello *et al.*, 2001; Peckmann *et al.*, 2002), and siderite of wetland paleosols (Ludvigson *et al.*, 1998, 2013). From this perspective, tubestones of the Pahuntoi bed of the Noonday Formation have isotopic covariance like pedogenic carbonate, but other dolomite in the Noonday Formation is uncorrelated like marine dolostones from which it was physically eroded.

Strong correlation of $\delta^{13}\text{C}$ and $\delta^{18}\text{O}$ in pedogenic carbonate is caused by selection for light isotopologues of CO_2 during photosynthesis on land (Farquhar & Cernusak, 2012; Broz *et al.*, 2021), unlike ocean or lakes with oxygen of water vastly in excess of carbon (Retallack, 2016). Correlation is related to stomatal conductance and fractionation by enzymes such as rubisco (Retallack, 2016), and carbonic anhydrase (Chen *et al.*, 2018), because $\delta^{13}\text{C}$ and $\delta^{18}\text{O}$ covariance is seen in respired soil CO_2 (Ehleringer & Cook, 1998; Ehleringer *et al.*, 2000), and in plant cellulose (Barbour & Farquhar, 2000; Barbour *et al.*, 2002). These Cambrian and Ediacaran paleosols predate the evolution of stomates (Retallack, 2022), so enzymatic control is more likely responsible for observed covariance in stable isotopes of pedogenic carbonate older than Ordovician (Fig. 9A). The covariance is not affected by metamorphism to greenschist facies in paleosols of the Juniata and Bloomsburg formations (Fig. 9A; Retallack, 2015a, b), so is unlikely to have been altered for the Noonday Formation.

Ravinement surfaces

A notable feature of the Noonday Formation is the Radcliff Member (Pettersen *et al.*, 2011), an intraformational ravinement surface with relief of 200 m and a very distinct heterogeneous fill of red, white and black breccia, sandstone, and shale (Creveling *et al.*, 2016). This heterogeneous fill of the Radcliff Member basal facies (formerly known as “Ibex Formation” of Corsetti & Kaufman, 2003) contrasts with uniform dolomitic tubestones of the Sentinel Peak and Mahogany Flats Members (Creveling *et al.*, 2016). The boundary between the two facies, includes narrow canyon-like features (Fig. 1). This was a large erosional feature, but was it a continental shelf with submarine canyons, or an upland with valleys above a lowland, like the modern Chinese Loess Plateau (Fig. 10)?

Upper submarine fan and canyon facies are generally coarse-grained breccias, conglomerates and cross bedded sandstones passing outwards and distally into turbidites (Howell & Link, 1979; Morris & Busby-Spera, 1990), different from the largely silty Noonday Formation basal facies, which lacks shaley tails to rare graded-beds (Creveling *et al.*, 2016). Submarine canyons also tend to be orthogonal to the coast (Twitchell & Roberts, 1982; Normark *et al.*, 2009; Jobe *et al.*, 2011), and not at a marked angle to the slope as in Noonday Formation paleovalleys (Fig. 1).

Red paleokarst filled with dolostone breccia (Paka beds) is evidence that the Sentinel Peak and Mahogany Flats Members were uplands rather than a submerged carbonate platform or ramp (Creveling *et al.*, 2016). Further evidence for this view includes the within-bed chemical differentiation, granulometry, crystal fans, sheeted cracks, carbonate shrubs, and stable isotopic correlation outlined in previous paragraphs, and comparison with Quaternary loess. Well known loess units such as the Peoria Loess of North America are generally less than 20 m thick and contain few paleosols (Bettis *et al.*, 2003; Wang *et al.*, 2006; Retallack, 2011), but the 252 m thick and geographically extensive Noonday Formation with numerous paleosols (Fig. 3) is more like the Chinese Loess Plateau (Fig. 10). By this modern analogy, the Noonday Formation platform facies can be considered comparable with upland Gansu, and the basal facies (Fig. 1) comparable with lowland Hunan, Hubei and Henan (Sun, 2002). Calcareous loess of China is about 180 m thick with 35 successive Pleistocene paleosols (Sun *et al.*, 2010). Ravinement surfaces like that of the Radcliff Member are also found within Chinese loess (Liu & Chang, 1962). Large scale cross bedding in Galena Canyon outcrops (Cloud *et al.*, 1974) is similar to paleodunes in Chinese loess (Sun *et al.*, 2010).

Alternatively, the Noonday Formation has been interpreted as a marine carbonate platform with submarine canyons and dissecting the platform edge (Creveling *et al.*, 2016), but that interpretation is not supported by petrographic, geochemical, granulometric, and crystallographic observations of the previous paragraphs. Carbonate shrubs in the Noonday Formation have been attributed to encrusting and interstitial marine microbial films (Fraiser & Corsetti, 2003), but careful examination of these features presented in the following paragraphs reveals much greater size and complexity than known in microbial films (Guido *et al.*, 2016; Heim *et al.*, 2017; Scopelliti & Russo, 2021). Neither field, petrographic, geochemical, nor fossil evidence support interpretation of the Noonday Formation as marine.

EDIACARAN FOSSIL LICHEN

Tubestones of the Noonday Formation have been regarded as fluid escape structures (Cloud *et al.*, 1974; Kennedy *et al.*, 2001; Bosak *et al.*, 2010) or as unusual inverted stromatolites (Corsetti & Grotzinger, 2005), but

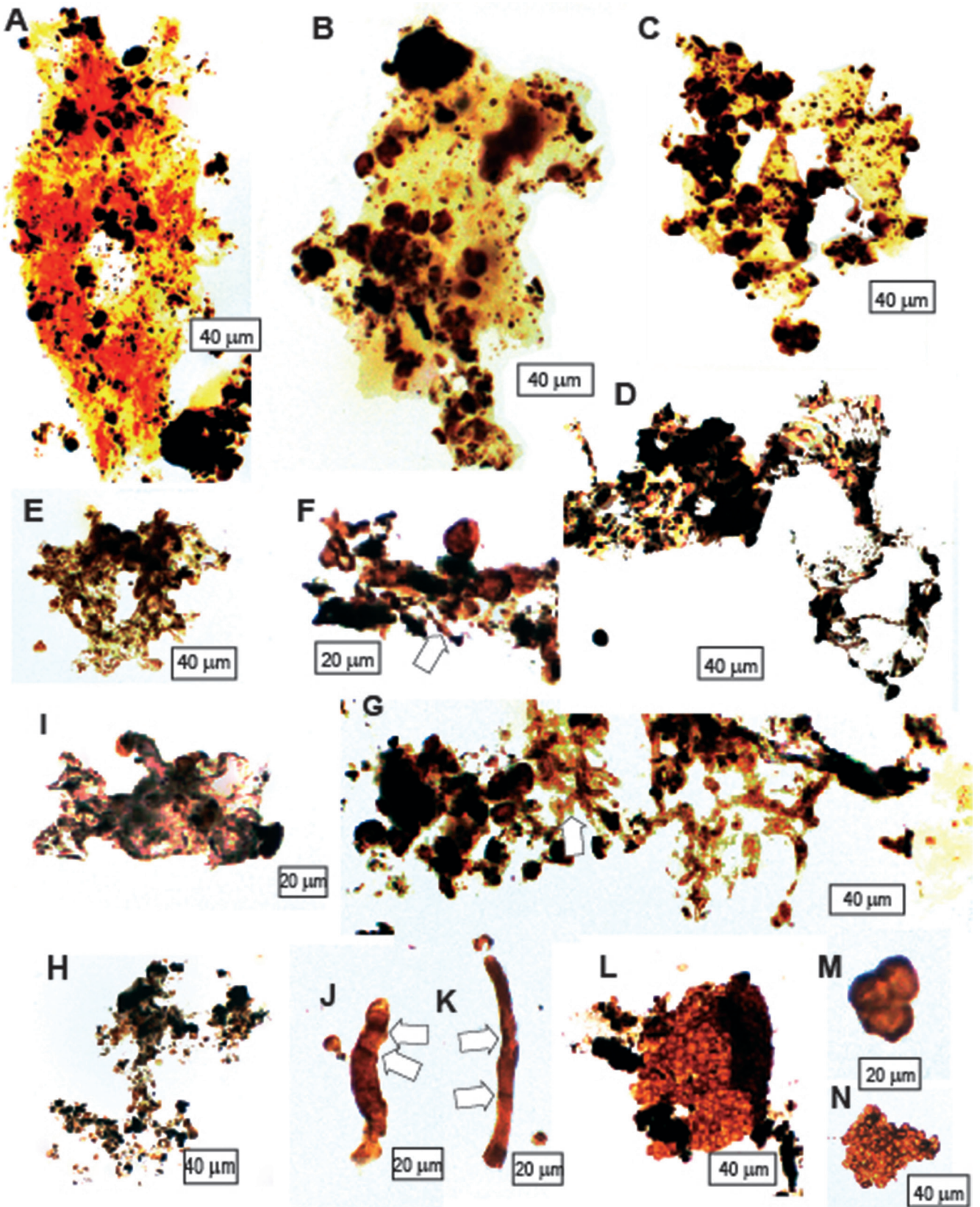


Fig. 14—*Ganarake scalaris* gen et sp. nov. from macerated palynological preparation. (A–C, E, H) thalli with oval to spheroidal photobionts; (D) septate stolon with fans of thallus; (F–G) hyphae and attached spheroidal photobionts of algal layer (Y hyphal junctions at arrows); (I) rhizines; (J–K) septate hyphae (septae at arrows); (L) partial sporangium; (M–N) spore masses. England finder coordinates on slide F11611 are: (A) R39/3; (B) W21/2; (C) D43/4; (D) R44/3; (E) D16/1; (F) S46/3; (G) V26/1; (H) Q44/2; (I) O12/3; (J) T38/4; (K) J16/4; (L) U37/2; (M) S11/4; (N) G11/3.

a variety of histological details are evidence for a third hypothesis that they were lichens. Noonday Formation as non-marine loess is compatible with the idea that the tubestones were lichenized fungi in growth position, because lichens are mostly terrestrial, with few taxa tolerant of constant immersion (Hawksworth, 2000). *Ganarake scalaris* gen et sp nov. is not quite tubular, but a stack of cup-shaped bodies (Fig. 11C–E), vertical to bedding (Fig. 11A), with a central crystalline core (Fig. 11B). They are 25.7 ± 4.3 (17.7–32.0) mm in diameter (Fig. 12) and can be as long as the 1 m thickness of Pahuntoi beds (Fig. 3). They are vertical like plumb-bobs, even in low angle cross beds (Hoffman, 2011). In thin section the cups contain delicate, fractally branching organic structures (Fig. 13E–H), often copiously overgrown with needle fiber calcite (Fig. 13C), radiating from an open cavity with isopachous dolomite cement (Fig. 13A–C). These mineral overgrowths are evidence that the organic branching structures were indigenous to the rocks, and overgrown during soil formation. Additional evidence that the fossils grew in Pahuntoi paleosols is the highly correlated $\delta^{13}\text{C}$ and $\delta^{18}\text{O}$ of these carbonate overgrowths (Fig. 9). Contamination of the palynological macerates (Figs 14, 15) by other fossils from tubestone matrix is possible, but unlikely because the limited array of structures revealed by maceration of a single silicified tubestone was also seen in place within thin sections (Fig. 13). Contamination by modern fungi and microbes also is possible, but ruled out by the dark color of all the fossils due to burial diagenesis (brown and black series of Yule *et al.*, 2000).

Fungal histology

Fungal affinities are apparent from a variety of microscopic observations, as also noted for Ediacaran fungi described by Gan *et al.* (2021). Macerated organic remains of *Ganarake* have a stratified thallus with four distinct layers: (1) upper cortex rectangular to cubic cells (Fig. 14D, 15A, 15I), (2) layer with spheroidal cells punctured by and enveloped by slender hyphae (Fig. 15E–I), (3) medulla of loose hyphae (Fig. 15I), and (4) lower cortex a few cells thick, elaborated at intervals into multicellular rhizines extending downward from the base (Fig. 15I). This thallus complexity rules out lichenized Actinobacteria (Kalakoutskii *et al.*, 1990). Other fungal features of *Ganarake* are aseptate hyphae, showing Y and H branching (Fig. 14G), and hyphal fusion into ladder-like forms (Fig. 13J). Also found were short lengths of septate hyphae (Fig. 14J–K), instances of bulging cells between hyphal septae (Fig. 15K), and aggregation of small spheroidal cells (Fig. 14L–N). The septate hyphae were also observed at the base of foliose thalli (Fig. 14D), and may have formed initials around the central cavity. Bulging cells between hyphae (Fig. 15K) may have been serial zygospores, but appear deformed as if artefacts of twisting. The isolated septate hyphae and bulging cells are attributed to *Ganarake*, because found in palynological preparation of a single

Ganarake specimen, though they could be fragments of other fossils accidentally included. Large spheroidal cells within a matrix of slender hyphae, and both punctured by and encircled by hyphae (Figs 13A–D, 14F–H), are likely coccoidal photobionts. Of different origin are dense aggregations of small spheroidal cells (Fig. 14L–N) interpreted as spores within a spherical sporangium, which judging from preserved peridial curvature was 350 μm in diameter. A plausible explanation for the central hollow of *Ganarake* is that it was filled with truffle-like masses of sporangia, not preserved due to decay or germination. The central hollow is filled with sparry dolomite, in part after oxalate also apparent from crystal form. Bipyrnidal skeletal acicular needles like those of fungal oxalate are commonly encountered within the thallus (Fig. 15B–E).

Spherical cells punctured and encircled by hyphae (Figs 14F–G, 15D–J) are interpreted as lichen photobionts. The biological nature of the photobiont is not well constrained by $\delta^{13}\text{C}$ isotopic composition of organic matter in Noonday tubestones, which is -21.27 ± 2.54 ‰ (n=8 from (Corsetti & Kauffman, 2003), like both cyanobacteria (–8 to –35 ‰ $\delta^{13}\text{C}$) and algae (–3 to –28 ‰ $\delta^{13}\text{C}$ (Schidlowski, 2001)). The size of spheroidal photobionts is 10 to 29 μm , larger than usual for cyanobacteria, and more like eukaryotic algae (Schopf, 1991). Algal photobionts within lichen associations are commonly only 10 μm in diameter when freshly released from the lichen, but grow to 25 μm soon after (Ahmadjian, 1967; Henley *et al.*, 2004).

Ganarake is the oldest known ectosymbiotic lichenized fungus, but was neither basidiomycotan or ascomycotan like modern lichens (Lücking & Nelsen, 2018), though preceded by 2.2 Ga *Diskagma*, which has been compared with the living glomeromycotan, endocyanotic *Geosiphon* (Retallack *et al.*, 2013). Other Proterozoic Glomeromycota are represented by vesicles of *Tappania* as old as 1.5 Ga (Retallack, 2015c). Other Ediacaran mucoromycotan or glomeromycotan fungi associated with spherical cells are from geologically younger stratigraphic levels than *Ganarake* (Gan *et al.*, 2021; Yuan *et al.*, 2005). Although mucoromycotan affinities are plausible, there is no living fungus exactly like *Ganarake*.

Window lichen nabkhas

Ganarake was ecologically similar to Fensterflechten (“window lichens”), first recognized in Namibia (Vogel, 1955) for *Eremastrella crystallinum*. Window lichens are squamulose ascomycotan lichens at the surface of the soil with a thick upper cortex cracked into translucent, crystal-like structures which allow light to penetrate to the algal layer deeper in the soil where it is protected from desiccation but prone to sediment cover (Fig. 16). Window lichens have multihyphal rhizines up to 1 mm diameter, penetrating 5 mm down into the soil. Window lichens are now known from Chile (Follmann, 1965), China (Yang & Wei, 2008), and Crete

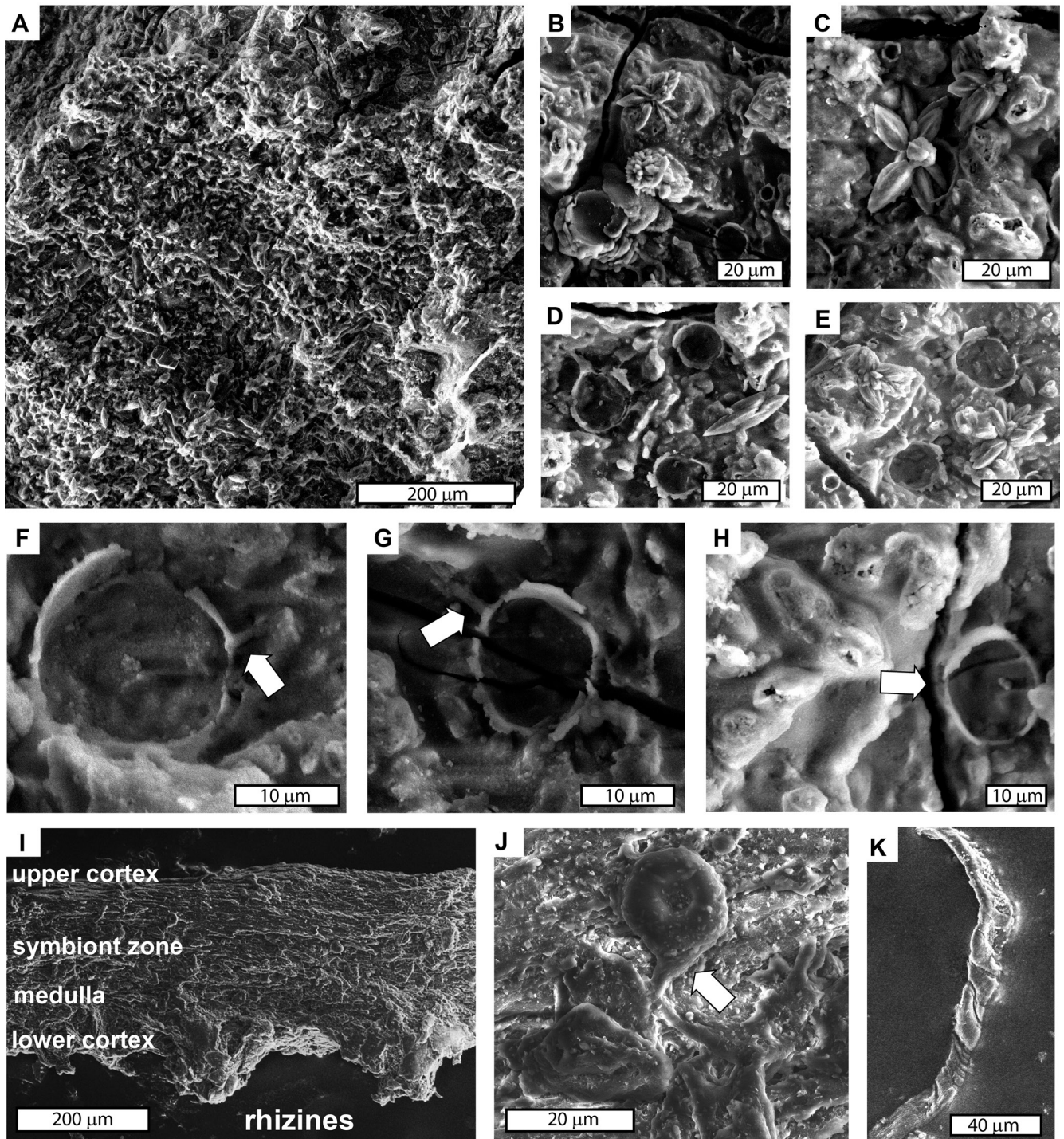


Fig. 15—*Ganarake scalaris* gen et sp. nov. scanning electron microscope images of acid etched slab (A–H) and macerated organic matter (I–K). (A) thallus with spheroidal photobionts; (B) skeletal dipyramidal acicular crystals of calcite after oxalate and etched spheroidal cells; (C–H) spheroidal cells with attached hyphae; (I) cross section of thallus with upper cortex above photobiont layer and lower cortex extending down into multicellular rhizoids; (J) indented spheroidal photobionts with attached and anastomosing hyphae; (K) hypha with possible zygosporangia or twist damage. Arrows indicate haustorial attachments of hyphae.

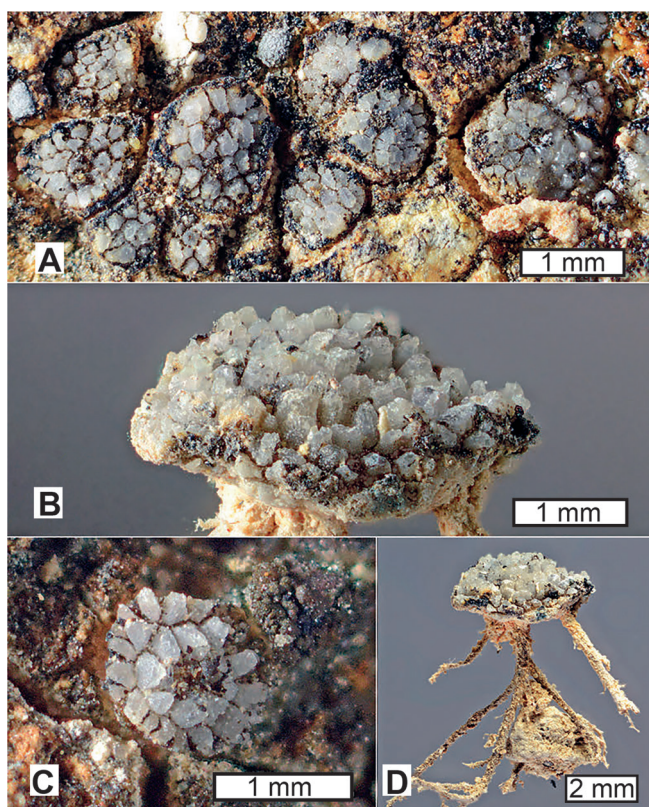


Fig. 16—Modern window lichen (“Fensterflechte”) *Endocarpon crystallinum* (Verrucariaceae, Ascomycota), from Istro, Crete. Fine crystalline pruina is present, but the large grey structures are semitransparent cortex rather than crystals. (A) view down onto ground; (B) older squamule; (C) young squamule; (D) squamule and thallus with substrate removed, showing attachment rhizines. Scale bars are 1 and 2 mm. This lichen is unrelated to the fossil, but has an external form comparable with that envisaged for *Ganarake*. Reproduced from Timdal (2017) with permission of Einar Timdal and Volker Otte.

(Timdal, 2017). Their transparent upper cortical cracks give the appearance of crystals, but *Ganarake* had actual crystals, later dolomitized, which may have focused light onto the algal layer in a thallus that was prone to cover by aggrading sediment. Comparison of the growth form of *Ganarake* with *Eremastrella* does not extend to taxonomic identification. There are no ascomycotan features visible in *Ganarake*, which is an unrelated problematic fossil more likely related to Mucoromycota or Glomeromycota.

The domed structure of the Galena Canyon tubestone outcrop (Fig. 2B) was first noted by Cloud *et al.* (1974) and interpreted as a giant stromatolite. On originally dipping flanks of the structure tubestones remain perpendicular like plumb-bobs, and interpreted as vertical growth of geoplumb stromatolites within the larger dome (Hoffman, 2011).

By the loess model proposed here, a better comparison is with nabkhas, a widely used term for dunes that form around clumps of plants, also called coppice dunes, redbou, phytogenic hillocks, and bush mounds (Nickling & Wolfe, 1994). Well documented examples are nabkhas around salt tree (*Nitraria retusa*) in Kuwait (Khalaf & Al-Awadi, 2012), mesquite (*Prosopis juliflora*) in New Mexico (Langford, 2000; Parsons *et al.*, 2003), and anu (*Leptadenia hastata*) in Mali (Nickling & Wolfe, 1994). These vertically growing woody shrubs and vines act as a baffle for sediment that piles into dunes 1–2 m high and 5–10 m long. This scale is comparable with the tubestones of Galena Canyon, and allows reinterpretation of the “giant stromatolite” of Cloud *et al.* (1974) as a lichen nabkha. No large domed structures were seen around tubestones in the exposures around Noonday Mine, but the tubestones do seem to have kept pace with eolian accumulation. Nevertheless, a lichen like *Ganarake* had much less biomass and no above-ground leaves compared with modern examples of nabkha dunes, and was more like window lichens.

Ganarake scalaris is envisioned as a window lichen growing upward with sediment accretion like a nabkha and lichen stromatolite (Fig. 17). On the soil surface it was a radial array of foliose, dichotomously branching thalli around a central cavity of reproductive truffles and oxalate crystals. These thalli included an upper and lower cortex with an intervening algal layer, and had basal rhizines. The whole structure was encrusted with needle fiber calcite and oxalate crystals which anchored it within the loose silt matrix. The radiating ring of thalli was buried by accretion of an eolian lamina, but then formed another ring on the newly deposited surface. Orientation to light explains the plumb-bob attitude of tubes within aggrading Pahuntoi paleosols, but some lateral migration was observed near the top of the bed, perhaps due to slowed rate of sediment accumulation.

SYSTEMATIC PALEONTOLOGY

FUNGI Moore, 1980

MUCOROMYCOTA? Doweld, 2001

FAMILY *INCERTAE SEDIS*

Ganarake gen. nov.

<https://www.mycobank.org/MB/843123>

(Figs 11–15)

Type species—*Ganarake scalaris* sp. nov.

Diagnosis—Successive, stacked, shallow, bowl-shaped, hypogeous thalli, formed from pinnately and dichotomously

branching foliose thalli radiating in all directions about 10 mm from around a central hollow 5 mm in diameter; foliose thalli with upper and lower cortex, central symbiont zone, lower medulla, and basal multicellular rhizines; hyphae mostly aseptate, with wider septate hyphae around the central hollow giving rise to foliose thalli; photobiont spherical to ovoid, indented by appressoria and haustoria of aseptate hyphae; sporocarps spherical with thousands of small spherical to ovoid spores and a thin peridium.

Etymology—This genus is named in honor of Tian Gan, discover of comparable Ediacaran fungi (Gan *et al.*, 2021), combined with Greek *arake* (f.) for bowl.

Description—Tubestone is a misnomer for these fossils because they are a series of shallow, irregular cups stacked one on top of another and about 20 mm in diameter (Figs 11–12). This is one reason why they were not regarded as fluid escape structures, nor metazoan burrows, root traces, solution pipes, columnar stromatolites, or spaces between stromatolites (Cloud *et al.*, 1974). The cups branch from a wide central hollow, perhaps originally empty, but now filled with sparry dolomite (Fig. 13A–C). The cup shaped flanges are formed by radially arranged foliose thalli branching both pinnately and dichotomously from septate hyphae and expanding outward to define the shallow cups (Figs 13E–I; 14A–D, 14H). The organic thalli are extensively overgrown with oxalate and carbonate crystals (Fig. 13A–D), and their remnants appear like ropes in thin section (Fig. 13E–I), but the thalli are flattened foliose structures in macerates (Fig. 14A–H), and in scanning electron micrographs (Fig. 15A). The foliose cortical layer consists of rectangular to cubic cells (Figs 14D, 15A, 15I). Below the upper cortical layer is a layer of spheroidal cells, punctured by and enveloped by slender hyphae (Fig. 15I). Spheroids concentrated within a particular layer are seen in a surface with upper cortex removed (Fig. 15A). Below the layer with spheroids attached by haustorial hyphae (Fig. 15E–H) is a zone of loose hyphae and with fewer spheroids regarded as a medulla (Fig. 15I). Below that again is a lower cortex a few cells thick, elaborated at intervals into multicellular rhizines extending downward from the base (Fig. 15I). Many thalli are not well preserved, but degraded and narrowed by overgrowth of needle fiber calcite (Figs 13D, 15B–E). Small spheroids in clusters (Fig. 14L–M) are interpreted as spores, and the dark tissue on the outer margin of one cluster (Fig. 14M) is regarded as a peridium of a sporocarp.

Comparisons—Only a single species of *Ganarake* is known, but other Ediacaran fossils may prove to be related species. Noonday Formation tubestones have been compared with stromatolites, acknowledging that they differ fundamentally as concave-up laminae (Corsetti & Grotzinger, 2005). The various fractally branching structures of the Noonday Formation have also been compared with “marine carbonate shrubs”, such as *Frutexites* (Fraiser & Corsetti, 2003), but have a more complex structure of internally

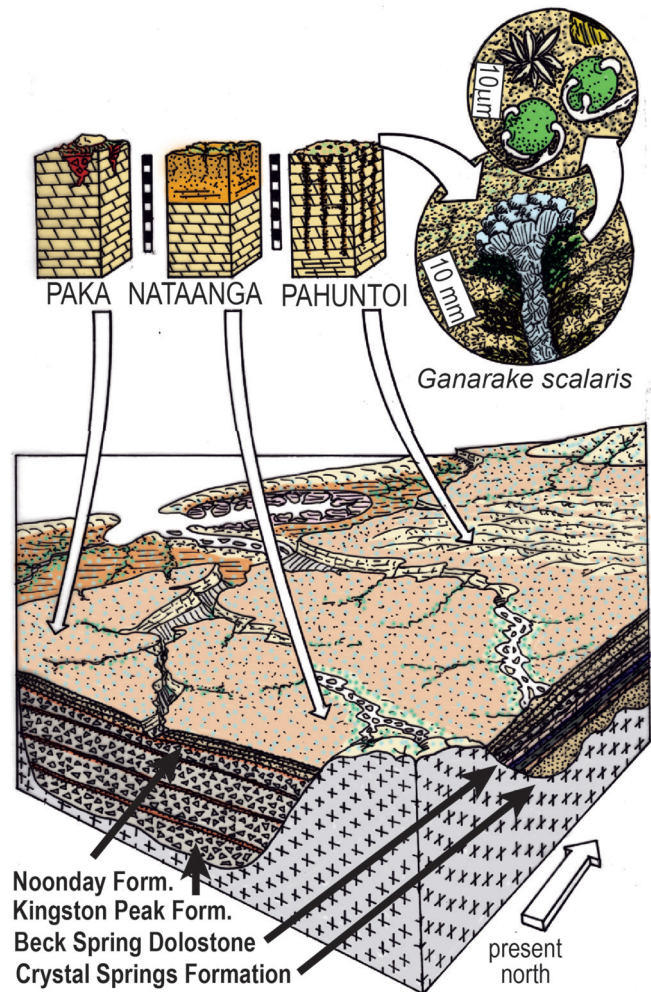


Fig. 17—Reconstructed early Ediacaran landscape, paleosols, and fossils of Death Valley, California. Cutaway enlargement of *Ganarake* shows vertical section of cups around central tube below and surface expression above, with photobiont and oxalate details in upper enlargement.

differentiated multicellular thalli then *Frutexites* (Figs 13–15). Genuine *Frutexites* has the appearance of pyrolusite dendrites of fractally arranged small crystals, induced by activity of unicellular iron–manganese oxidizing bacteria (Guido *et al.*, 2016; Heim *et al.*, 2017; Scopelliti & Russo, 2021), but opaque grains are rare in the Noonday Formation. *Ganarake* lacks the histology of fossil calcareous algae, the box-like cells of rhodophytes, the verticillate structure of dasyclads, and the loose fountaining structure of chlorophytes (Wray, 1977; Flügel, 1977). Spheroids from Cryogenian siltstones of the Elatina Formation in South Australia (Le Heron *et al.*, 2016) differ from *Ganarake* by lacking hyphal connections and much larger diameter (200–500 µm). An unnamed Ediacaran lichen from phosphorites of the Ediacaran Doushantou Formation of China (Yuan *et al.*, 2005), has spheroidal and

tubular cells, but not arranged within a recognizable thallus. Another unnamed fungus from paleocaves in “caprock” of the Ediacaran Doushantou Formation of China has both hyphae and spheroidal cells, but they are not intimately connected, nor organized into a thallus structure (Gan *et al.*, 2021).

Palynological investigations of Ediacaran marine rocks yield a great diversity of “acritarchs” and occasional cell aggregates, interpreted as communities of plankton, nekton, algae, cyanobacteria, and fungi (Zang & Walter, 1989; Grey, 2005; Agić *et al.*, 2019). In contrast, palynological preparation of a silicified piece of tubestone for this study found only four different kinds of organic fossils: sheets of cells with attached large spheroids, narrow aseptate tubular cells, wide septate tubular cells, and clusters of small spheroids (Fig. 14). Rather than a community of diverse unicellular organisms, this assemblage is interpreted here as different parts and life stages of a single multicellular organism.

Remarks—The biological affinities of *Ganarake* are uncertain, like other problematic Precambrian fungal fossils (Yuan *et al.*, 2005; Retallack *et al.*, 2013; Gan *et al.*, 2021). Mucoromycota include largely aseptate, but occasionally septate, hyphae, like *Ganarake* (Hibbett *et al.*, 2007). There are some similarities with pea truffles of the order Endogonales, and Family Endogonaceae, such as *Endogone*, which form ectomycorrhizal symbioses with a variety of land plants including liverworts, hornworts, ferns, lycopsids, conifers and angiosperms (Yao *et al.*, 1996; Desirò *et al.*, 2017). *Endogone* forms macroscopic truffles of spores within hyphal envelopes somewhat like those found with *Ganarake*. *Endogone* however differs greatly in its diffuse mycelium, rather than fractally branched lichenized thalli with internal cortical–medullary differentiation of *Ganarake*, convergent with ascomycotan and basidiomycotan lichens (Ahmadjian, 1967; Henley *et al.*, 2004). Although thallus organization of *Ganarake* is similar to dikaryan (Ascomycota + Basidiomycota) lichens, *Ganarake* has mainly aseptate hyphae, and lacks clamp connections and ascospores. The oldest known dikaryan lichens and fungi are early Devonian (415 Ma: Honegger *et al.*, 2013).

Ganarake scalaris sp. nov.

<https://www.mycobank.org/MB/843137>

(Figs 11–15)

Type specimen—Specimen F116111A (Fig. 11C) in Condon Collection of the Museum of Natural and Cultural History of the University of Oregon in Eugene.

Etymology—The specific epithet is from Latin *scalaris*, of a ladder.

Measurements—Widths of megafossil specimens are 25.7 ± 4.3 (17.7–32.0) mm, formatted mean \pm one standard deviation (range) on the flanges, and 13.9 ± 3.2 mm (9.4–

22.8) on the narrow waists (n=29). Mean diameter of 500 examples from Galena Canyon is 16.4 ± 4.4 (4.0–39.6) mm. Their lengths can be up to 1 m long within individual beds. Individual foliose thalli are 244 ± 31 (205–282) μm thick (n=5), but highly variable in width 62 ± 34 (5–147) μm (n=24). Basal podetial cords are 24 ± 2 (22–28) μm in diameter (n=6). Cortical cells are 38 ± 18 (10–73) μm long by 13 ± 5 (5–26) μm wide (n=36). Aseptate hyphae of the photobiont zone are 3 ± 1 (1–5) μm in diameter (n=5) and spheroidal photobionts are 15 ± 3 (7–29) μm in diameter (n=72). There also are basal septate hyphae 13 ± 2 (10–15) μm in diameter (n=18). Rhizoids are 55 ± 26 (31–93) μm in diameter (n=6). Masses of 8 to 194 spores are in masses 25 to 164 μm across in palynological preparation. The largest fragment has an external curvature, which if projected would give a circular mass of thousands of spores some 350 μm in diameter. The spores are spheroidal to oval, 8.4 ± 1.6 (4–14) μm in diameter (n=63), and have walls 1.9 ± 0.6 (1–3) μm thick (n=63). Oxalate skeletal bipyramidal crystals are 14.3 ± 3.5 (10–23) μm long (n=30), and 5.2 ± 1.4 (3–7) μm wide (n=30).

Remarks—*Ganarake* was an extinct organism somewhat similar to living *Endogone*, but distinct in forming a stratified lichen thallus unknown in *Endogone* or Endogonaceae (Yao *et al.*, 1996; Desirò *et al.*, 2017). Pea truffles of *Endogone* formed from spore clusters may be an explanation for the central hollow of *Ganarake* filled with dolomitized calcite and oxalate. These spores may have dispersed or rotted to leave the central hollow that was propagated as a tube as it grew up through eolian sediment accretion. This mode of growth is comparable with lichen stromatolites which are irregularly laminar calcretes from successive crustose lichens on limestone (Klappa, 1979) or silcrete ministromatolites from small fruticose lichens on sandstone (Gorbushina *et al.*, 2001). Stromatolites or depression between stromatolites were early explanations for Noonday tubestones (Cloud *et al.*, 1974; Corsetti & Grotzinger, 2005), which can no longer explain the foliose thalli and microstructures documented here.

CONCLUSIONS

Previous studies have assumed that the Noonday Formation and its enigmatic tubestones were a tropical marine “cap carbonate” deposited on glacial tillites, a paleoclimatic swing of a magnitude without any modern analog (Hoffman, 2011). Boron and calcium isotope anomalies also showed that marine deposition required an 1.1 pH unit shift in the world ocean, which is incredible for such a large volume of water (Kasemann *et al.*, 2005, 2010). A variety of observations detailed here suggest instead that the Noonday Formation was a sequence of paleosols: within-bed petrographic and chemical differentiation; common silicate minerals, loess-like grain size and textures, sheet cracks, needle fiber calcite, oxalate crystal, light YREE enrichment, carbon and oxygen stable isotopic covariation, intraformational red paleokarst

breccias, and ravinement surfaces. In soils and paleosols pH changes several units from horizon to horizon (Retallack & Burns, 2016; Lukens *et al.*, 2018). Three distinct kinds of bed here named Pahuntui, Paka and Nataanga (Shoshoni Language Project, 2019) can be identified as Psamment, Orthent and Ochrept soils (Soil Survey Staff, 2014). A plausible modern analog for such cap carbonates is calcareous loess on Pleistocene tills (Retallack, 2011). The Quaternary Chinese Loess Plateau has a sequence of paleosols, thickness and paleogeographic distribution (Sun *et al.*, 2004) comparable with the Noonday Formation (Williams *et al.*, 1974).

Silicified tubestones of the Noonday Formation contain permineralized cellular details of *Ganarake scalaris* gen et sp. nov., with aseptate hyphae showing Y and H shaped branching, and ladder-like arrays from hyphal fusion. Large sporangia and possible deformed zygospores are most like those of living *Endogone* (Mucoromycota: Yao *et al.*, 1996). Unlike the mycorrhizal living *Endogone*, *Ganarake* had dichotomously branching foliose thalli with upper and lower cortex and central algal zone with large spheroidal cells showing haustorial connection of a lichen. The spheroidal photobiont has the diameter ($15 \pm 3 \mu\text{m}$, range $7\text{--}29 \mu\text{m}$) and organic carbon isotopic composition (organic $\delta^{13}\text{C} - 21.27 \pm 2.54 \text{‰}$: Corsetti & Kaufman, 2003) of living chlorophyte alga, which are $10\text{--}25 \mu\text{m}$ in size (Schopf, 1991) and $-24.3 \pm 6.4 \text{‰}$ $\delta^{13}\text{C}$ composition (Retallack & Landing, 2014). Chlorophytic symbionts of lichens are smaller than free living forms (Ahmadjian, 1967; Henley *et al.*, 2004) and the isotopic composition of fungi is the same as their food source (Boyce *et al.*, 2007; Hobbie & Boyce, 2010). The foliose thallus grew in whorls around a central cavity filled with sparry carbonate and oxalate in the manner of modern window lichens (Timdal, 2017), growing new whorls above the old after cover by eolian laminae to form geoplumb tubes through aggrading loess.

Acknowledgements—*Galena Canyon was visited under U.S. National Park permit DEVA-2008-SCI-0034. Kurt Langworthy and Julie Barkman aided with scanning electron microscopy. Lauren Wright, Bennie Troxel, Tian Gan, Shuhai Xiao, Paul Hoffman, and Bruce Runnegar offered useful discussion. Work was supported by the Sandal Society of the Museum of Natural and Cultural History of the University of Oregon.*

REFERENCES

- Agić H, Högström AE, Moczyłowska M, Jensen S, Palacios T, Meinhold G, Ebbestad JOR, Taylor WL & Høyberget M 2019. Organically-preserved multicellular eukaryote from the early Ediacaran Nyborg Formation, Arctic Norway. *Nature Scientific Reports* 9: 1–12, <https://doi.org/10.1038/s41598-019-50650-x>.
- Ahm ASC, Maloof AC, Macdonald FA, Hoffman PF, Bjerrum CJ, Bold U, Rose CV, Strauss JV & Higgins JA 2019. An early diagenetic deglacial origin for basal Ediacaran “cap dolostones”. *Earth and Planetary Science Letters* 506: 292–307, <https://doi.org/10.1016/j.epsl.2018.10.046>.
- Ahmadjian V 1967. A guide to the algae occurring as lichen symbionts: isolation, culture, cultural physiology and identification. *Phycologia* 6: 127–160, <https://doi.org/10.2216/i0031-8884-6-2-127.1>.
- Aiello IW, Garrison RE, Moore EC, Kastner M & Stakes DS 2001. Anatomy and origin of carbonate structures in a Miocene cold-seep field. *Geology* 29: 1111–1114, [https://doi.org/10.1130/0091-7613\(2001\)029<1111:AAOCS>2.0.CO;2](https://doi.org/10.1130/0091-7613(2001)029<1111:AAOCS>2.0.CO;2).
- Aubert D, Stille P & Probst A 2001. REE fractionation during granite weathering and removal by waters and suspended loads: Sr and Nd isotopic evidence. *Geochimica & Cosmochimica Acta* 65: 387–406, [https://doi.org/10.1016/S0016-7037\(00\)00546-9](https://doi.org/10.1016/S0016-7037(00)00546-9).
- Bajnóczi B & Kovács-Kis V 2006. Origin of pedogenic needle-fiber calcite revealed by micromorphology and stable isotope composition—a case study of a Quaternary paleosol from Hungary. *Geochemistry* 66: 203–212, <https://doi.org/10.1016/j.chemer.2005.11.002>.
- Barbour MM & Farquhar GD 2000. Relative humidity- and ABA-induced variation in carbon and oxygen isotope ratios of cotton leaves. *Plant, Cell and Environment* 23: 473–485, <https://doi.org/10.1046/j.1365-3040.2000.00575.x>.
- Barbour MM, Walcroft AS & Farquhar GD 2002. Seasonal variation in $\delta^{13}\text{C}$ and $\delta^{18}\text{O}$ of cellulose from growth rings of *Pinus radiata*. *Plant, Cell and Environment* 25: 1483–1499, <https://doi.org/10.1046/j.0016-8025.2002.00931.x>.
- Barfod GH, Albarède F, Knoll AH, Xiao S, Télouk P, Frei R & Baker J 2002. New Lu–Hf and Pb–Pb age constraints on the earliest animal fossils. *Earth and Planetary Science Letters* 201: 203–212, [https://doi.org/10.1016/S0012-821X\(02\)00687-8](https://doi.org/10.1016/S0012-821X(02)00687-8).
- Bathurst RGC 1970. Problems of lithification in carbonate muds. *Proceedings of the Geologists' Association* 81: 429–440, [https://doi.org/10.1016/S0016-7878\(70\)80005-0](https://doi.org/10.1016/S0016-7878(70)80005-0).
- Batten DJ 1999. Small palynomorphs. *In*: Jones TP & Rowe NP (Editors) – Fossil plants and spores: modern techniques. London: Geological Society of London, 15–19.
- Bau M 1996. Controls on the fractionation of isoivalent trace elements in magmatic and aqueous systems: evidence from Y/Ho, Zr/Hf, and lanthanide tetrad effect. *Contributions to Mineralogy and Petrology* 123: 323–333, <https://doi.org/10.1007/s004100050159>.
- Bestland EA, Retallack GJ, Rice AE & Mindszenty A 1996. Late Eocene detrital laterites in central Oregon: mass balance geochemistry, depositional setting and landscape evolution. *Geological Society of America Bulletin* 108: 285–302, [https://doi.org/10.1130/0016-7606\(1996\)108<0285:LEDLIC>2.3.CO;2](https://doi.org/10.1130/0016-7606(1996)108<0285:LEDLIC>2.3.CO;2).
- Bettis EA, Mason JP, Swinehart JB, Miao X & Roberts HM 2003. Cenozoic eolian sedimentary systems of the USA mid-continent. *In*: Easterbook DJ (Editor)–Quaternary Geology of the United States: INQUA 2003 Field Guide Volume. Reno, Desert Research Institute, 195–218.
- Bolhar R & Van Kranendonk MJ 2007. A non-marine depositional setting for the northern Fortescue Group, Pilbara Craton, inferred from trace element geochemistry of stromatolitic carbonates. *Precambrian Research* 155: 229–250, <https://doi.org/10.1016/j.precamres.2007.02.002>.
- Bosak T, Bush J, Flynn M, Liang B, Ono S, Sim MS, & Petroff AP 2010. Formation and stability of oxygen rich bubbles that shape photosynthetic mats. *Geobiology* 8: 45–55, <https://doi.org/10.1111/j.1472-4669.2009.00227.x>.
- Boyce CK, Hotton CL, Fogel ML, Cody GD, Hazen RM, Knoll AH & Hueber FM 2007. Devonian landscape heterogeneity recorded by a giant fungus. *Geology* 25: 399–402, <https://doi.org/10.1130/G23384A.1>.
- Brimhall GH, Chadwick OA, Lewis CJ, Compston W, Williams IS, Danti KJ, Dietrich WE, Power ME, Hendricks D & Bratt J 1992. Deformational mass transport and invasive processes in soil evolution. *Science* 255: 695–702, <https://doi.org/10.1126/science.255.5045.695>.
- Broz A, Retallack GJ, Maxwell TM & Silva LC 2021. A record of vapour pressure deficit preserved in wood and soil across biomes. *Scientific Reports* 11: 1–12, <https://doi.org/10.1038/s41598-020-80006-9>.
- Butterfield NJ 2015. The Neoproterozoic. *Current Biology* 25: 859–863, <https://doi.org/10.1016/j.cub.2015.07.021>.
- Carlisle D, Davis DL, Kildale MB & Stewart RM 1954. Base metal and iron deposits of southern California. *In*: Jahns RH (Editor) – Geology of southern California. California Division of Mines Bulletin 1: 41–49.

- Caxito FA, Frei R, Uhlein GJ, Dias TG, Ártig TB & Uhlein A 2018. Multiproxy geochemical and isotope stratigraphy records of a Neoproterozoic Oxygenation Event in the Ediacaran Sete Lagoas cap carbonate, Bambuí Group, Brazil. *Chemical Geology* 481: 119–132, <https://doi.org/10.1016/j.chemgeo.2018.02.007>.
- Chadwick OA, Brimhall GH & Hendricks DM 1990. From a black to a gray box—a mass balance interpretation of pedogenesis. *Geomorphology* 3: 369–390, [https://doi.org/10.1016/0169-555X\(90\)90012-F](https://doi.org/10.1016/0169-555X(90)90012-F).
- Chen S, Gagnon AC & Adkins JF 2018. Carbonic anhydrase, coral calcification and a new model of stable isotope vital effects. *Geochimica & Cosmochimica Acta* 236: 179–197, <https://doi.org/10.1016/j.gca.2018.02.032>.
- Church SE, Cox DP, Wooden JL, Tingley JV & Vaughn RB 2005. Base- and precious-metal deposits in the Basin and Range of southern California and southern Nevada—Metallogenic implications of lead isotope studies. *Earth-Science Reviews* 73: 323–346, <https://doi.org/10.1016/j.earscirev.2005.04.012>.
- Cloud PE, Wright LA, Williams EG, Diehl P & Walter MR 1974. Giant stromatolites and associated vertical tubes from the Upper Proterozoic Noonday Dolomite, Death Valley region, eastern California. *Geological Society of America Bulletin* 85: 1869–1882, [https://doi.org/10.1130/0016-7606\(1974\)85<1869:GSAAVT>2.0.CO;2](https://doi.org/10.1130/0016-7606(1974)85<1869:GSAAVT>2.0.CO;2).
- Condon D, Zhu M, Bowring S, Wang W, Yang A & Jin Y 2005. U–Pb ages from the Neoproterozoic Doushantuo Formation, China. *Science* 308: 95–98, <https://doi.org/10.1126/science.1107765>.
- Corsetti FA & Grotzinger JP 2005. Origin and significance of tube structures in Neoproterozoic post-glacial cap carbonates: example from Noonday Dolomite, Death Valley, United States. *Palaios* 20: 348–362, <https://doi.org/10.2110/palo.2003.p03-96>.
- Corsetti FA & Kaufman AJ 2003. Stratigraphic investigations of carbon isotope anomalies and Neoproterozoic ice ages in Death Valley, California. *Geological Society of America Bulletin* 115: 916–932, <https://doi.org/10.1130/B25066.1>.
- Corsetti FA & Kaufman AJ 2005. The relationship between the Neoproterozoic Noonday Dolomite and the Ibex Formation: new observations and their bearing on ‘Snowball Earth’. *Earth-Science Reviews* 73: 63–78, <https://doi.org/10.1016/j.earscirev.2005.07.002>.
- Creveling JR & Mitrovica JX 2014. The sea-level fingerprint of a Snowball Earth deglaciation. *Earth and Planetary Science Letters* 399: 74–85, <https://doi.org/10.1016/j.epsl.2014.04.029>.
- Creveling JR, Bergmann KD & Grotzinger JP 2016. Cap carbonate platform facies model, Noonday Formation, SE California. *Geological Society of America Bulletin* 128: 1249–1269, <https://doi.org/10.1130/B31442.1>.
- Dalrymple RW, Narbonne GM & Smith L 1985. Eolian action and the distribution of Cambrian shales in North America. *Geology* 13: 607–610, [https://doi.org/10.1130/0091-7613\(1985\)13<607:EAATDO>2.0.CO;2](https://doi.org/10.1130/0091-7613(1985)13<607:EAATDO>2.0.CO;2).
- Derbyshire E 2001. Geological hazards in loess terrain, with particular reference to the loess regions of China. *Earth-Science Reviews* 54: 231–260, [https://doi.org/10.1016/S0012-8252\(01\)00050-2](https://doi.org/10.1016/S0012-8252(01)00050-2).
- Desirò A, Rimington WR, Jacob A, Pol NV, Smith ME, Trappe JM, Bidartondo MI & Bonito G 2017. Multigene phylogeny of Endogonales, an early diverging lineage of fungi associated with plants. *IMA Fungus* 8: 245–257, <https://doi.org/10.5598/ima fungus.2017.08.02.03>.
- Doweld A 2001. *Prosyllabus tracheophytorum tentamen systematis plantarum vascularium (Tracheophyta)* 80: 1–110.
- Driese SG, Jirsa MA, Ren M, Brantley SL, Sheldon ND, Parker D & Schmitz M 2011. Neoproterozoic paleoweathering of tonalite and metabasalt: Implications for reconstructions of 2.69 Ga early terrestrial ecosystems and paleoatmospheric chemistry. *Precambrian Research* 189: 1–17, <https://doi.org/10.1016/j.precamres.2011.04.003>.
- Ehleringer JR & Cook CS 1998. Carbon and oxygen isotope ratios of ecosystem respiration along an Oregon conifer transect: preliminary observations based on small flask sampling. *Tree Physiology* 18: 513–519, <https://doi.org/10.1093/treephys/18.8-9.513>.
- Ehleringer JR, Buchmann N & Flanagan LB 2000. Carbon isotope ratios in belowground carbon cycle processes. *Ecological Applications* 10: 412–422, [https://doi.org/10.1890/1051-0761\(2000\)010\[0412:CIRIBC\]2.0.CO;2](https://doi.org/10.1890/1051-0761(2000)010[0412:CIRIBC]2.0.CO;2).
- Evans DAD & Raub TD 2011. Neoproterozoic glacial palaeolatitudes: A global update. *In: Arnaud E, Halverson GP & Shields-Zhou G (Editors) – The Geological Record of Neoproterozoic Glaciations*. Geological Society of London Memoir 36: 93–112, <https://doi.org/10.1144/M36.7>.
- Farquhar GD & Cernusak LA 2012. Ternary effects on the gas exchange of isotopologues of carbon dioxide. *Plant, Cell and Environment* 35: 1221–1231, <https://doi.org/10.1111/j.1365-3040.2012.02484.x>.
- Fisk HN 1951. Loess and Quaternary geology of the Lower Mississippi Valley. *Journal of Geology* 59: 333–356, <https://doi.org/10.1086/625872>.
- Flügel E 1977. *Fossil algae: Recent results and developments* Berlin, Berlin, 375 p.
- Follmann G 1965. *Fensterflechten in der Atacamawüste*. *Naturwissenschaften* 52: 434–435, <https://doi.org/10.1007/BF00589697>.
- Food & Agriculture Organization 1974. *Soil Map of the World. Vol. 1 Legend*. Paris, UNESCO, 205 p.
- Fraiser ML & Corsetti FA 2003. Neoproterozoic carbonate shrubs: interplay of microbial activity and unusual environmental conditions in post-Snowball Earth oceans. *Palaios* 18: 378–387, [https://doi.org/10.1669/0883-1351\(2003\)018<0378:NCSIOM>2.0.CO;2](https://doi.org/10.1669/0883-1351(2003)018<0378:NCSIOM>2.0.CO;2).
- Gan T, Luo T, Pang K, Zhou C, Zhou G, Wan B, Li G, Yi Q, Czaja AD & Xiao S 2021. Cryptic terrestrial fungus-like fossils of the early Ediacaran Period. *Nature Communications* 12: 1–12, <https://doi.org/10.1038/s41467-021-20975-1>.
- Gorbushina AA, Boettcher M, Krumbein WE & Vendrell-Saz M 2001. Biogenic forsterite and opal as a product of biodeterioration and lichen stromatolite formation in table mountain systems (tepuis) of Venezuela. *Geomicrobiology Journal* 18: 117–132, <https://doi.org/10.1080/01490450151079851>.
- Grey K 2005. Ediacaran palynology of Australia. *Memoir Association of Australasian Palaeontologists* 31: 1–439.
- Grimley DA, Follmer LR & McKay ED 1998. Magnetic susceptibility and mineral zonations controlled by provenance in loess along the Illinois and central Mississippi River valleys. *Quaternary Research* 49: 24–36, <https://doi.org/10.1006/qres.1997.1947>.
- Guido A, Rosso A, Sanfilippo R, Russo F & Mastandrea A 2016. *Frutexitis* from microbial/metazoan bioconstructions of recent and Pleistocene marine caves (Sicily, Italy). *Palaeogeography, Palaeoclimatology, Palaeoecology* 453: 127–138, <https://doi.org/10.1098/rspb.2010.0201>.
- Hartl WP, Klapper H, Barbier B, Ensikat HJ, Dronskowski R, Müller P, Ostendorf G, Tye A, Bauer R & Barthlott W 2007. Diversity of calcium oxalate crystals in Cactaceae. *Botany* 85: 501–517, <https://doi.org/10.1139/B07-046>.
- Hawksworth DL 2000. Freshwater and marine lichen-forming fungi. *Fungal Diversity* 5: 1–7, https://www.fungaldiversity.org/fdp/sfdp/FD_5_1-7.pdf.
- Hayes JL, Riebe CS, Holbrook WS, Flinchum BA & Hartsough PC 2019. Porosity production in weathered rock: Where volumetric strain dominates over chemical mass loss. *Science Advances* 5(9): eaao0834, <https://doi.org/10.1126/sciadv.aao0834>.
- He R, Jiang G, Lu W & Lu Z 2020. Iodine records from the Ediacaran Doushantuo cap carbonates of the Yangtze Block, South China. *Precambrian Research* 347: 105843, <https://doi.org/10.1016/j.precamres.2020.105843>.
- Heim C, Quéric NV, Ionescu D, Schäfer N & Reitner J 2017. *Frutexitis*–like structures formed by iron oxidizing biofilms in the continental subsurface (Åspö Hard Rock Laboratory, Sweden). *PLoS One* 12: e0177542, <https://doi.org/10.1371/journal.pone.0177542>.
- Henley WJ, Hironaka JL, Guillou L, Buchheim MA, Buchheim JA, Fawley MW & Fawley KP 2004. Phylogenetic analysis of the ‘*Nannochloris*–like’ algae and diagnoses of *Picochloris oklahomensis* gen. et sp. nov. (Trebouxiophyceae, Chlorophyta). *Phycologia* 43: 641–652, <https://doi.org/10.2216/i0031-8884-43-6-641.1>.
- Hibbett DS, Binder M, Bischoff JF, Blackwell M, Cannon PF, Eriksson OE, Huhndorf S, James T, Kirk PM, Lücking R & Lumbsch HT 2007. A higher-level phylogenetic classification of the Fungi. *Mycological Research* 111: 509–547, <https://doi.org/10.1016/j.mycres.2007.03.004>.

- Hobbie EA & Boyce CK 2010. Carbon sources for the Palaeozoic giant fungus *Prototaxites* inferred from modern analogs. *Philosophical Transactions of the Royal Society of London B* 277: 2149–2156, <https://doi.org/10.1098/rspb.2010.0201>.
- Hoffman PF 2011. Strange bedfellows: glacial diamictite and cap carbonate from the Marinoan (635 Ma) glaciation in Namibia. *Sedimentology* 58: 57–119, <https://doi.org/10.1111/j.1365-3091.2010.01206.x>.
- Hoffman PF & Schrag DP 2002. The snowball Earth hypothesis: testing the limits of global change. *Terra Nova* 14: 129–155, <https://doi.org/10.1046/j.1365-3121.2002.00408.x>.
- Hoffman PF, Kaufman AJ, Halverson GP & Schrag DP 1998. A Neoproterozoic Snowball Earth. *Science* 281: 1342–1346, <https://doi.org/10.1126/science.281.5381.1342>.
- Honegger R, Edwards D & Axe L 2013. The earliest records of internally stratified cyanobacterial and algal lichens from the Lower Devonian of the Welsh Borderland. *New Phytologist* 197: 264–275, <https://doi.org/10.1111/nph.12009>.
- Hongo Y & Nozaki Y 2001. Rare earth element geochemistry of hydrothermal deposits and *Calyptogenia* shell from the Iheya Ridge vent field, Okinawa Trough. *Geochemical Journal* 35: 347–354, <https://doi.org/10.2343/geochemj.35.347>.
- Howell DG & Link MH 1979. Eocene conglomerate sedimentology and basin analysis, San Diego and the southern California borderland. *Journal of Sedimentary Research* 49: 517–539, <https://doi.org/10.1306/212F777F-2B24-11D7-8648000102C1865D>.
- Huang C–M, Wang C–S & Tang Y 2005. Stable carbon and oxygen isotopes of pedogenic carbonates in Ustic Vertisols: implications for paleoenvironmental change. *Pedosphere* 15: 539–544.
- Huang J, Chu X, Chang H & Feng L 2009. Trace element and rare earth element of cap carbonate in Ediacaran Doushantuo Formation in Yangtze Gorges. *Chinese Science Bulletin* 54: 3295–3302, <https://doi.org/10.1007/s11434-009-0305-1>.
- Jobe ZR, Lowe DR & Uchytel SJ 2011. Two fundamentally different types of submarine canyons along the continental margin of Equatorial Guinea. *Marine and Petroleum Geology* 28: 843–860, <https://doi.org/10.1016/j.marpetgeo.2010.07.012>.
- Kalakoutskii LV, Zenova GM, Soina VS & Likhacheva AA 1990. Associations of actinomycetes with algae. *Actinomycetes* 1: 27–42, <https://tspace.library.utoronto.ca/html/1807/21221/ac90006.html>.
- Kasemann SA, Hawkesworth CJ, Prave AR, Fallick AE & Pearson PN 2005. Boron and calcium isotope composition in Neoproterozoic carbonate rocks from Namibia: evidence for extreme environmental change. *Earth and Planetary Science Letters* 231: 73–86, <https://doi.org/10.1016/j.epsl.2004.12.006>.
- Kasemann SA, Prave AR, Fallick AE, Hawkesworth CJ & Hoffmann KH 2010. Neoproterozoic ice ages, boron isotopes, and ocean acidification: Implications for a snowball Earth. *Geology* 38: 775–778, <https://doi.org/10.1130/G30851.1>.
- Kearsey T, Twitchett RJ & Newell AJ 2012. The origin and significance of pedogenic dolomite from the Upper Permian of the South Urals of Russia. *Geological Magazine* 149: 291–307, <https://doi.org/10.1017/S0016756811000926>.
- Kennedy K & Eyles N 2021. Syn-rift mass flow generated ‘tectonofacies’ and ‘tectonosequences’ of the Kingston Peak Formation, Death Valley, California, and their bearing on supposed Neoproterozoic panglacial climates. *Sedimentology* 68: 352–381, <https://doi.org/10.1111/sed.12781>.
- Kennedy MJ, Christie–Blick N & Sohl LE 2001. Are Proterozoic cap carbonates and isotopic excursions a record of gas hydrate destabilization following Earth’s coldest intervals? *Geology* 29: 443–446, [https://doi.org/10.1130/0091-7613\(2001\)029<0443:APCCAI>2.0.CO;2](https://doi.org/10.1130/0091-7613(2001)029<0443:APCCAI>2.0.CO;2).
- Khalaf FI & Al–Awadhi JM 2012. Sedimentological and morphological characteristics of gypsaceous coastal nabkhas on Bubiyan Island, Kuwait, Arabian Gulf. *Journal of Arid Environments* 82: 31–43, <https://doi.org/10.1016/j.jaridenv.2012.02.017>.
- Kirschvink JL 1991. Late Proterozoic low–latitude global glaciation: the snowball Earth. In: Schopf JW & Klein C (Editors). *The Proterozoic Biosphere: a multidisciplinary study*—Cambridge, Cambridge University Press, 51–52.
- Klappa CF 1979. Lichen stromatolites; criterion for subaerial exposure and a mechanism for the formation of laminar calcretes (caliche). *Journal of Sedimentary Research* 49: 387–400, <https://doi.org/10.1306/212F7752-2B24-11D7-8648000102C1865D>.
- Knauth LP, Brilli M & Klonowski S 2003. Isotope geochemistry of caliche developed on basalt. *Geochimica & Cosmochimica Acta* 67: 185–195, [https://doi.org/10.1016/S0016-7037\(02\)01051-7](https://doi.org/10.1016/S0016-7037(02)01051-7).
- Knoll AH 1985. Exceptional preservation of photosynthetic organisms in silicified carbonates and silicified peats. *Philosophical Transactions of the Royal Society of London. B, Biological Sciences* 311: 111–122, <https://doi.org/10.1098/rstb.1985.0143>.
- Knoll A, Walter M, Narbonne G & Christie–Blick N 2006. The Ediacaran Period: a new addition to the geologic time scale. *Lethaia* 39: 13–30, <https://doi.org/10.1080/00241160500409223>.
- Komar PD 1985. The hydraulic interpretation of turbidites from their grain sizes and sedimentary structures. *Sedimentology* 32: 395–407, <https://doi.org/10.1111/j.1365-3091.1985.tb00519.x>.
- Korsch RJ, Roser BP & Kamprad JL 1993. Geochemical, petrographic and grain–size variations within single turbidite beds. *Sedimentary Geology* 83: 15–35, [https://doi.org/10.1016/0037-0738\(93\)90180-D](https://doi.org/10.1016/0037-0738(93)90180-D).
- Kunzmann M, Halverson GP, Sossi PA, Raub TD, Payne JL & Kirby J 2013. Zn isotope evidence for immediate resumption of primary productivity after snowball Earth. *Geology* 41: 27–30, <https://doi.org/10.1130/G33422.1>.
- Lang Farmer G & Ball TT 1997. Sources of Middle Proterozoic to Early Cambrian siliciclastic sedimentary rocks in the Great Basin: A Nd isotope study. *Geological Society of America Bulletin* 109: 1193–1205, [https://doi.org/10.1130/0016-7606\(1997\)109<1193:SOMPTE>2.3.CO;2](https://doi.org/10.1130/0016-7606(1997)109<1193:SOMPTE>2.3.CO;2).
- Langford RP 2000. Nabkha (coppice dune) fields of south–central New Mexico, USA. *Journal of Arid Environments* 46: 25–41, <https://doi.org/10.1006/jare.2000.0650>.
- Le Heron DP, Alderton DHM, Collinson ME, Grassineau N, Sykes D & Trundle AE 2016. A eukaryote assemblage intercalated with Marinoan glacial deposits in South Australia. *Journal of the Geological Society London* 173: 560–568, <https://doi.org/10.1144/jgs2015-156>.
- Liu C, Wang Z, Raub TD, Macdonald FA & Evans DA 2014. Neoproterozoic cap–dolostone deposition in stratified glacial meltwater plume. *Earth and Planetary Science Letters* 404: 22–32, <https://doi.org/10.1016/j.epsl.2014.06.039>.
- Liu T–S & Chang T–H 1962. The loess of China. *Acta Geologica Sinica* 42: 1–14.
- Lohmann KG 1988. Geochemical patterns of meteoric diagenetic systems and their application to studies of paleokarst. In: James NP & Choquette PW (Editors) – *Paleokarst*. Berlin: Springer, 59–80, https://doi.org/10.1007/978-1-4612-3748-8_3.
- Long H, Lai Z, Fuchs M, Zhang J & Yang L 2012. Palaeodunes intercalated in loess strata from the western Chinese Loess Plateau: Timing and palaeoclimatic implications. *Quaternary International* 263: 37–45, <https://doi.org/10.1016/j.quaint.2010.12.030>.
- Long JS, Hu C, Robbins LL, Byrne RH, Paul JH & Wolny JL 2017. Optical and biochemical properties of a southwest Florida whiting event. *Estuarine, Coastal and Shelf Science* 96: 258–268, <https://doi.org/10.1016/j.ecss.2017.07.017>.
- Loyd SJ, Marengo PJ, Hagadorn JW, Lyons TW, Kaufman AJ, Sour–Tovar F & Corsetti FA 2012. Sustained low marine sulfate concentrations from the Neoproterozoic to the Cambrian: Insights from carbonates of northwestern Mexico and eastern California. *Earth and Planetary Science Letters* 339: 79–94, <https://doi.org/10.1016/j.epsl.2012.05.032>.
- Lücking R & Nelsen MP 2018. Ediacarans, Protolichens, and Lichen–Derived *Penicillium*: A critical reassessment of the evolution of lichenization in Fungi. In: Krings M, Harper CJ, Cuneo NR, & Rothwell GW (Editors) – *Transformative paleobotany: Papers to commemorate the life and legacy of Thomas N. Taylor*. London: Academic Press, 551–589, <https://doi.org/10.1016/B978-0-12-813012-4.00023-1>.
- Ludvigson GA, González LA, Metzger RA, Witzke BJ, Brenner RL, Murillo AP & White TS 1998. Meteoric sphaerosiderite lines and their use for

- paleohydrology and paleoclimatology. *Geology* 26: 1039–1042, [https://doi.org/10.1130/0091-7613\(1998\)026<1039:MSLATU>2.3.CO;2](https://doi.org/10.1130/0091-7613(1998)026<1039:MSLATU>2.3.CO;2).
- Ludvigson GA, González LA, Fowle DA, Roberts JA, Driese SG, Villarreal MA, Smith JJ, Suarez MB & Nordt LC 2013. Paleoclimatic applications and modern process studies of pedogenic siderite. *In: Driese SG & Nordt LC (Editors) – New Frontiers in Paleopedology and Terrestrial Paleoclimatology*. Society of Economic Paleontologists and Mineralogists Special Publication 104: 79–87, <https://doi.org/10.2110/sepmsp.104.01>.
- Lukens WE, Nordt LC, Stinchcomb GE, Driese SG & Tubbs JD 2018. Reconstructing pH of paleosols using geochemical proxies. *Journal of Geology* 126: 427–449, <https://doi.org/10.1086/697693>.
- MacDonald FA, Cohen PA, Dudás FÓ & Schrag DP 2010. Early Neoproterozoic scale microfossils in the lower Tindir Group of Alaska and the Yukon Territory. *Geology* 38: 143–146, <https://doi.org/10.1130/G25637.1>.
- Mahon RC, Dehler CM, Link PK, Karlstrom KE & Gehrels GE 2014. Detrital zircon provenance and paleogeography of the Pahrump Group and overlying strata, Death Valley, California. *Precambrian Research* 251: 102–117, <https://doi.org/10.1016/j.precamres.2014.06.005>.
- McFadden KA, Xiao S, Zhou C & Kowalewski M 2009. Quantitative evaluation of the biostratigraphic distribution of acanthomorphic acritarchs in the Ediacaran Doushantuo Formation in the Yangtze Gorges area, South China. *Precambrian Research* 173: 170–190, <https://doi.org/10.1016/j.precamres.2009.03.009>.
- McMahon WJ, Liu AG, Tindal BH & Kleinans MG 2020. Ediacaran life close to land: Coastal and shoreface habitats of the Ediacaran macrobiota, the Central Flinders Ranges, South Australia. *Journal of Sedimentary Research* 90: 1463–1499, <https://doi.org/10.2110/jsr.2020.029>.
- Mehmoud M, Yaseen M, Khan EU & Khan MJ 2018. Dolomite and dolomitization model—a short review. *International Journal of Hydrology* 2: 549–553, <https://doi.org/10.15406/ijh.2018.02.00124>.
- Melim LA, Swart PK & Eberli GP 2004. Mixing zone diagenesis in the subsurface of Florida and the Bahamas. *Journal of Sedimentary Research* 76: 904–913, <https://doi.org/10.1306/042904740904>.
- Minařík L, Žigová A, Bendl J, Skřivan P & Šťastný M 1998. The behaviour of rare-earth elements and Y during the rock weathering and soil formation in the Říčany granite massif, Central Bohemia. *Science of the Total Environment* 215: 101–111, [https://doi.org/10.1016/S0048-9697\(98\)00113-2](https://doi.org/10.1016/S0048-9697(98)00113-2).
- Minguez D, Kodama KP & Hillhouse JW 2015. Paleomagnetic and cyclostratigraphic constraints on the synchronicity and duration of the Shuram carbon isotope excursion, Johnnie Formation, Death Valley Region, CA. *Precambrian Research* 266: 395–408, <https://doi.org/10.1016/j.precamres.2015.05.033>.
- Moore RT 1980. Taxonomic proposals for the classification of marine yeasts and other yeast-like fungi including the smuts. *Botanica Marina* 23: 361–373.
- Morris W & Busby–Spera C 1990. A submarine–fan valley–levee complex in the Upper Cretaceous Rosario Formation: Implication for turbidite facies models. *Geological Society of America Bulletin* 102: 900–914, [https://doi.org/10.1130/0016-7606\(1990\)102<0900:ASFVLC>2.3.CO;2](https://doi.org/10.1130/0016-7606(1990)102<0900:ASFVLC>2.3.CO;2).
- Morton PK 1965. *Geology of the Queen of Sheba Lead Mine: Death Valley, California*. California Division of Mines and Geology Special Report 88: 1–18.
- Minamoto T, Solongo T, Okuyama A, Fukushi K, Yunden A, Batbold T, Altansukh O, Takahashi Y, Iwai H & Nagao S 2020. Rare earth element distributions in rivers and sediments from the Erdenet Cu–Mo mining area, Mongolia. *Applied Geochemistry* 123: 104800, <https://doi.org/10.1016/j.apgeochem.2020.104800>.
- Murphy CP 1983. Point counting pores and illuvial clay in thin section. *Geoderma* 31: 133–150, [https://doi.org/10.1016/0016-7061\(83\)90004-6](https://doi.org/10.1016/0016-7061(83)90004-6).
- Nelson LL, Smith EF, Hodgins EB, Crowley JL, Schmitz MD & MacDonald FA 2020. Geochronological constraints on Neoproterozoic rifting and onset of the Marinoan glaciation from the Kingston Peak Formation in Death Valley, California (USA). *Geology* 48: 1083–1087, <https://doi.org/10.1016/10.1130/G47668.1>.
- Newberry R 1987. Use of intrusive and calc–silicate compositional data to distinguish contrasting skarn types in the Darwin polymetallic skarn district, California, USA. *Mineralium Deposita* 22: 207–215, <https://doi.org/10.1007/BF00206612>.
- Newberry RJ, Einaudi MT & Eastman HS 1991. Zoning and genesis of the Darwin Pb–Zn–Ag skarn deposit, California; a reinterpretation based on new data. *Economic Geology* 86: 960–982, <https://doi.org/10.2113/gsecongeo.86.5.960>.
- Nickling WG & Wolfe SA 1994. The morphology and origin of nabkhas, region of Mopti, Mali, West Africa. *Journal of Arid Environments* 28: 13–30, [https://doi.org/10.1016/S0140-1963\(05\)80017-5](https://doi.org/10.1016/S0140-1963(05)80017-5).
- Normark WR, Piper DJ, Romans BW, Covault JA, Dartnell P, Sliter RW & Lee HJ 2009. Submarine canyon and fan systems of the California Continental Borderland. *In: Lee HJ & Normark WR (Editors) – Earth Science in the Urban Ocean: The Southern California Continental Borderland*. Geological Society of America Special Paper 454: 141–168, [https://doi.org/10.1130/2009.2454\(2.7\)](https://doi.org/10.1130/2009.2454(2.7)).
- Novoselov AA & de Souza Filho CR 2015. Potassium metasomatism of Precambrian paleosols. *Precambrian Research* 262: 67–83, <https://doi.org/10.1016/j.precamres.2015.02.024>.
- Nugteren G, Van den Berghe J, van Huissteden JK & Zhisheng A 2004. A Quaternary climate record based on grain size analysis from the Luochuan loess section on the Central Loess Plateau, China. *Global and Planetary Change* 41: 167–218, <https://doi.org/10.1016/j.gloplacha.2004.01.004>.
- Ohnemüller F, Prave AR, Fallick AE & Kasemann SA 2014. Ocean acidification in the aftermath of the Marinoan glaciation. *Geology* 42: 1103–1106, <https://doi.org/10.1130/G35937.1>.
- Parsons AJ, Wainwright J, Schlesinger WH & Abrahams AD 2003. The role of overland flow in sediment and nitrogen budgets of mesquite dunefields, southern New Mexico. *Journal of Arid Environments* 53: 61–71.
- Peckmann J, Goedert JL, Thiel V, Michaelis W & Reitner J 2002. A comprehensive approach to the study of methane-seep deposits from the Lincoln Creek Formation, western Washington State, USA. *Sedimentology* 49: 855–873, <https://doi.org/10.1046/j.1365-3091.2002.00474.x>.
- Peterson R, Prave AR, Wernicke BP & Fallick AE 2011. The Neoproterozoic Noonday Formation, Death Valley region, California. *Geological Society of America Bulletin* 123: 1317–1336, <https://doi.org/10.1130/B30281.1>.
- Peterson R, Prave AR, Wernicke BP & Fallick AE 2013. The Neoproterozoic Noonday Formation, Death Valley region, California: Reply. *Geological Society of America Bulletin* 125: 252–255, <https://doi.org/10.1130/B30700.1>.
- Prave AR 1999. Two diamictites, two cap carbonates, two $\delta^{13}\text{C}$ excursions, two rifts: the Neoproterozoic Kingston Peak Formation, Death Valley, California. *Geology* 27: 339–342, [https://doi.org/10.1130/0091-7613\(1999\)027<0339:TDTCCCT>2.3.CO;2](https://doi.org/10.1130/0091-7613(1999)027<0339:TDTCCCT>2.3.CO;2).
- Pye K & Sherwin D 1999. Loess. *In: Goudie AS, Livingstone I & Stokes E (Editors) – Aeolian Environments, Sediments and Landforms*. Chichester, Wiley, 239–259, <https://doi.org/10.1086/625870>.
- Reesink AJH, Best J, Freiburg JT, Webb ND, Monson CC & Ritz RW 2020. Interpreting pre-vegetation landscape dynamics: The Cambrian Lower Mount Simon Sandstone, Illinois, USA. *Journal of Sedimentary Research* 90: 1614–1641, <https://doi.org/10.2110/jsr.2020.71>.
- Retallack GJ 1991. *Miocene paleosols and ape habitats of Pakistan and Kenya*. New York, Oxford University Press, 346 p.
- Retallack GJ 1997. *A colour guide to paleosols*. Wiley, Chichester, 175 p.
- Retallack GJ 2005. Pedogenic carbonate proxies for amount and seasonality of precipitation in paleosols. *Geology* 33: 333–336, <https://doi.org/10.1130/G21263.1>.
- Retallack GJ 2011. Neoproterozoic loess and limits to Snowball Earth. *Journal of the Geological Society of London* 168: 289–308, <https://doi.org/10.1144/0016-76492010-051>.
- Retallack GJ 2013. Ediacaran life on land. *Nature* 493: 89–92, <https://doi.org/10.1038/nature11777>.
- Retallack GJ 2015a. Late Ordovician glaciation initiated by early land plant evolution, and punctuated by greenhouse mass-extinctions. *Journal of Geology* 123: 509–538, <https://doi.org/10.1086/683663>.
- Retallack GJ 2015b. Silurian vegetation stature and density inferred from fossil soils and plants in Pennsylvania, USA. *Journal of the Geological*

- Society London 172: 693–709, <https://doi.org/10.1144/jgs2015-022>.
- Retallack GJ 2015c. Acritarch evidence of a late Precambrian adaptive radiation of Fungi. *Botanica Pacifica* 4: 19–33, <https://doi.org/10.17581/bp.2015.04203>.
- Retallack GJ 2016. Field and laboratory tests for recognition of Ediacaran paleosols. *Gondwana Research* 36: 94–110, <https://doi.org/10.1016/j.gr.2016.05.001>.
- Retallack GJ 2020. Boron paleosalinity proxy for deeply buried Paleozoic and Ediacaran fossils. *Palaeogeography Palaeoclimatology Palaeoecology* 540: 109536, <https://doi.org/10.1016/j.palaeo.2019.109536>.
- Retallack GJ 2021. Zebra rock and other Ediacaran paleosols from Western Australia. *Australian Journal of Earth Sciences* 68: 532–556, <https://doi.org/10.1080/08120099.2020.1820574>.
- Retallack GJ 2022. Ordovician–Devonian lichen canopies before evolution of woody trees. *Gondwana Research* 106: 211–223, <https://doi.org/10.1016/j.gr.2022.01.010>.
- Retallack GJ & Broz AP 2020. *Arumberia* and other Ediacaran–Cambrian fossils of central Australia. *Historical Biology* 32: 1964–1988, <https://doi.org/10.1080/08912963.2020.1755281>.
- Retallack GJ & Burns SF 2016. The effects of soil on the taste of wine. *GSA Today* 26(5): 4–9, <https://doi.org/10.1130/GSATG260A.1>.
- Retallack GJ & Landing E 2014. Affinities and architecture of Devonian trunks of *Prototaxites loganii*. *Mycologia* 106: 1143–1158, <https://doi.org/10.3852/13-390>.
- Retallack GJ & Mindszenty A 1994. Well preserved late Precambrian paleosols from northwest Scotland. *Journal of Sedimentary Research* 64: 264–281, <https://doi.org/10.1306/D4267D7A-2B26-11D7-8648000102C1865D>.
- Retallack GJ, Krull ES, Thackray GD & Parkinson D 2013. Problematic urn-shaped fossils from a Paleoproterozoic (2.2 Ga) paleosol in South Africa. *Precambrian Research* 235: 71–87, <https://doi.org/10.1016/j.precamres.2013.05.015>.
- Retallack GJ, Marconato A, Osterhout JT, Watts KE & Bindeman IN 2014. Revised Wonoka isotopic anomaly in South Australia and Late Ediacaran mass extinction. *Journal of the Geological Society London* 171: 709–722, <https://doi.org/10.1144/jgs2014-016>.
- Retallack GJ, Broz AP, Lai LSH & Gardner K 2021a. Neoproterozoic marine chemostratigraphy, or eustatic sea level change? *Palaeogeography, Palaeoclimatology, Palaeoecology* 562: 110155, <https://doi.org/10.1016/j.palaeo.2020.110155>.
- Retallack GJ, Chen Z-Q, Huan Y & Feng HY 2021b. Mesoproterozoic alluvial paleosols of the Ruyang Group in Henan, China. *Precambrian Research* 364: 106361, <https://doi.org/10.1016/j.precamres.2021.106361>.
- Schidlowski M 2001. Carbon isotopes as biogeochemical recorders of life over 3.8 Ga of Earth history: evolution of a concept. *Precambrian Research* 106: 117–134, [https://doi.org/10.1016/S0301-9268\(00\)00128-5](https://doi.org/10.1016/S0301-9268(00)00128-5).
- Schopf JW 1991. Proterozoic prokaryotes: affinities, geologic distribution, and evolutionary trends. In: Schopf JW & Klein C (Editors) – *The Proterozoic Biosphere: a multidisciplinary study*. Cambridge: Cambridge University Press, 195–218.
- Scopelliti G & Russo V 2021. Petrographic and geochemical characterization of the Middle–Upper Jurassic Fe–Mn crusts and mineralizations from Monte Inici (north-western Sicily): genetic implications. *International Journal of Earth Sciences* 110: 559–582, <https://doi.org/10.1007/s00531-020-01971-0>.
- Scotese CR 2021. An atlas of Phanerozoic paleogeographic maps: the seas come in and the seas go out. *Annual Review of Earth and Planetary Sciences* 49: 679–728, <https://doi.org/10.1146/annurev-earth-081320-064052>.
- Sheldon ND & Retallack GJ 2001. Equation for compaction of paleosols due to burial. *Geology* 29: 247–250, [https://doi.org/10.1130/0091-7613\(2001\)029<0247: EFCOPD>2.0.CO;2](https://doi.org/10.1130/0091-7613(2001)029<0247: EFCOPD>2.0.CO;2).
- Sheldon ND & Tabor NJ 2009. Quantitative paleoenvironmental and paleoclimatic reconstruction using paleosols. *Earth Science Reviews* 95: 1–52, <https://doi.org/10.1016/j.earscirev.2009.03.004>.
- Shoshoni Language Project 2019. Website: shoshoniproject.utah.edu, accessed December 31, 2019.
- Soil Survey Staff 2014. *Keys to Soil Taxonomy*. Washington DC: Natural Resources Conservation Service, 358 p.
- Sondi I & Juračić M 2010. Whiting events and the formation of aragonite in Mediterranean Karstic Marine Lakes: new evidence on its biologically induced inorganic origin. *Sedimentology* 57: 85–95, <https://doi.org/10.1111/j.1365-3091.2009.01090.x>.
- Stace HCT, Hubble GD, Brewer R, Northcote KH, Sleeman JR, Mulcahy MJ & Hallsworth EG 1968. *A handbook of Australian soils*. Adelaide, Rellim, 435 p.
- Sturm EV, Frank–Kamenetskaya O, Vlasov D, Zelenskaya M, Sazanova K, Rusakov A & Kniep R 2015. Crystallization of calcium oxalate hydrates by interaction of calcite marble with fungus *Aspergillus niger*. *American Mineralogist* 100: 2559–2565, <https://doi.org/10.2138/am-2015-5104>.
- Sugahara H, Sugitani K, Mimura K, Yamashita F & Yamamoto K 2010. A systematic rare-earth elements and yttrium study of Archean cherts at the Mount Goldsworthy greenstone belt in the Pilbara Craton: Implications for the origin of microfossil-bearing black cherts. *Precambrian Research* 177: 73–87, <https://doi.org/10.1016/j.precamres.2009.10.005>.
- Sun D, Bloemendal J, Rea DK, An Z, Vandenberghe J, Lu H, Su R & Liu T 2004. Bimodal grain-size distribution of Chinese loess, and its palaeoclimatic implications. *Catena* 55: 325–334, [https://doi.org/10.1016/S0341-8162\(03\)00109-7](https://doi.org/10.1016/S0341-8162(03)00109-7).
- Sun J 2002. Provenance of loess material and formation of loess deposits on the Chinese Loess Plateau. *Earth and Planetary Science Letters* 203: 845–859, [https://doi.org/10.1016/S0012-821X\(02\)00921-4](https://doi.org/10.1016/S0012-821X(02)00921-4).
- Sun Y, An Z, Clemens SC, Bloemendal J & Vandenberghe J 2010. Seven million years of wind and precipitation variability on the Chinese Loess Plateau. *Earth and Planetary Science Letters* 297: 525–535, <https://doi.org/10.1016/j.epsl.2010.07.004>.
- Surge DM, Savarese M, Dodd JR & Lohmann KC 1997. Carbon isotopic evidence for photosynthesis in Early Cambrian oceans. *Geology* 25: 503–506, [https://doi.org/10.1130/0091-7613\(1997\)025<0503: CIEFPI>2.3.CO;2](https://doi.org/10.1130/0091-7613(1997)025<0503: CIEFPI>2.3.CO;2).
- Swineford A & Frye JC 1951. Petrography of the Peoria loess in Kansas. *Journal of Geology* 59: 306–322, <https://doi.org/10.1086/625870>.
- Talbot MR 1990. A review of the palaeohydrological interpretation of carbon and oxygen isotopic ratios in primary lacustrine carbonates. *Chemical Geology Isotope Geoscience Section* 80: 261–279, [https://doi.org/10.1016/0168-9622\(90\)90009-2](https://doi.org/10.1016/0168-9622(90)90009-2).
- Taylor SR & McLennan SM 1985. *The continental crust: its composition and evolution*. Oxford, Blackwell, 312 p.
- Thompson JB, Schultze–Lam S, Beveridge TJ & Des Marais DJ 1997. Whiting events: biogenic origin due to the photosynthetic activity of cyanobacterial picoplankton. *Limnology and Oceanography* 42: 133–141, <https://doi.org/10.4319/lo.1997.42.1.0133>.
- Timdal E 2017. *Endocarpon crystallinum* found in Crete, a window-lichen new to Europe. *Herzogia* 30: 309–312, <https://doi.org/10.13158/hea.30.1.2017.309>.
- Torsvik TH & Cocks LRM 2013. Gondwana from top to base in space and time. *Gondwana Research* 24: 999–1030, <https://doi.org/10.1016/j.gr.2013.06.012>.
- Turland NJ, Wiersma JH, Barrie FR, Greuter W, Hawksworth DL, Herendeen PS, Knapp S, Kusber WH, Li DZ, Marhold K, May TW, McNeill J, Monro AM, Prado J, Price MJ & Smith GF 2018. International code of nomenclature for algae, fungi, and plants (Shenzhen Code) adopted by the Nineteenth International Botanical Congress Shenzhen, China, July 2017. *Regnum Vegetabile*. 159: 1–254, <https://doi.org/10.12705/Code.2018>.
- Twitchell DC & Roberts DG 1982. Morphology, distribution, and development of submarine canyons on the United States Atlantic continental slope between Hudson and Baltimore Canyons. *Geology* 10: 408–412, [https://doi.org/10.1130/0091-7613\(1982\)10<408: MDADOS>2.0.CO;2](https://doi.org/10.1130/0091-7613(1982)10<408: MDADOS>2.0.CO;2).
- Veizer J, Ala D, Azmy K, Bruckschen P, Buhl D, Bruhn F, Carden GAF, Diener A, Ebneth S, Godderis Y, Jasper T, Korte C, Pawellek F, Podlaha OG & Strauss H 1999. $^{87}\text{Sr}/^{86}\text{Sr}$, $\delta^{13}\text{C}$ and $\delta^{18}\text{O}$ evolution of Phanerozoic seawater. *Chemical Geology* 161: 59–88, [https://doi.org/10.1016/S0009-2541\(99\)00081-9](https://doi.org/10.1016/S0009-2541(99)00081-9).
- Verrecchia EP & Verrecchia KE 1994. Needle-fiber calcite: a critical review and a proposed classification. *Journal of Sedimentary Research*

- 64: 650–664, <https://doi.org/10.1306/D4267E33-2B26-11D7-8648000102C1865D>.
- Vogel S 1955. Niedere “Fensterpflanzen” in der südafrikanischen Wüste. Eine ökologische Schilderung. *Beiträge Biologie Pflanzen* 31: 45–135.
- Wang H, Mason JA & Balsam WL 2006. The importance of both geological and pedological processes in control of grain size and sedimentation rates in Peoria Loess. *Geoderma* 136: 388–400, <https://doi.org/10.1016/j.geoderma.2006.04.005>.
- Wanless HR 1979. Limestone response to stress; pressure solution and dolomitization. *Journal of Sedimentary Research* 49: 437–462, <https://doi.org/10.1016/j.geoderma.2006.04.005>.
- Wernicke B, Axen GJ & Snow JK 1988. Basin and Range extensional tectonics at the latitude of Las Vegas, Nevada. *Geological Society of America Bulletin* 100: 1738–1757, [https://doi.org/10.1130/0016-7606\(1988\)100<1738:BARETA>2.3.CO;2](https://doi.org/10.1130/0016-7606(1988)100<1738:BARETA>2.3.CO;2).
- Williams EG, Wright LA & Troxel BW 1974. The Noonday Dolomite and equivalent stratigraphic units, southern Death Valley region, California. *In: Wright LA, Troxel BW, Williams EG, Roberts MT & Diehl PE (Editors)–Guidebook: Death Valley Region, California and Nevada*. Boulder: Geological Society of America, 73–77.
- Williams GE, Gostin VA, McKirdy DM & Preiss WV 2008. The Elatina glaciation, late Cryogenian (Marinoan Epoch), South Australia: sedimentary facies and palaeoenvironments. *Precambrian Research* 163: 307–331, <https://doi.org/10.1016/j.precamres.2007.12.001>.
- Wilson MJ, Jones D & Russell JD 1980. Glushinskite, a naturally occurring magnesium oxalate. *Mineralogical Magazine* 43: 837–840, <https://doi.org/10.1180/minmag.1980.043.331.02>.
- Wray JL 1977. *Calcareous Algae*. New York, Elsevier, 185 p.
- Wright LA, Troxel BW, Williams EG, Roberts MT & Diehl PE 1976. Precambrian sedimentary environments of the Death Valley region, eastern California: Geologic features of Death Valley, California. *California Division of Mines and Geology Special Report* 106: 7–15.
- Xiao SH & Narbonne GM 2020. The Ediacaran Period. *In: Gradstein FM, Ogg JG, Schmitz MD & Ogg GM (Editors) – Geologic Time Scale 2020*. Amsterdam: Elsevier, 521–561, <https://doi.org/10.1016/B978-0-12-824360-2.00018-8>.
- Yang J & Wei J–C 2008. The new lichen species *Endocarpon crystallinum* from semiarid deserts in China. *Mycotaxon* 106: 445–448.
- Yao Y–J, Pegler DN & Young TWK 1996. *Genera of Endogonales*. Kew: Royal Botanical Gardens, 229 p.
- Yasukawa K, Nakamura K, Fujinaga K, Machida S, Ohta J, Takaya Y & Kato Y 2015. Rare–earth, major, and trace element geochemistry of deep–sea sediments in the Indian Ocean: Implications for the potential distribution of REY–rich mud in the Indian Ocean. *Geochemical Journal* 49: 621–635, <https://doi.org/10.2343/geochemj.2.0361>.
- Yu W, Algeo TJ, Zhou Q, Du Y & Wang P 2020. Cryogenian cap carbonate models: A review and critical assessment. *Palaeogeography, Palaeoclimatology, Palaeoecology* 552: 109727, 109727. <https://doi.org/10.1016/j.palaeo.2020.109727>.
- Yuan X–L, Xiao S–H & Taylor TN 2005. Lichen–like symbiosis 600 million years ago. *Science* 308: 1017–1020, <https://doi.org/10.1126/science.1111347>.
- Yule BL, Roberts S & Marshall JEA 2000. The thermal evolution of sporopollenin. *Organic Geochemistry* 31: 859–870. [https://doi.org/10.1016/S0146-6380\(00\)00058-9](https://doi.org/10.1016/S0146-6380(00)00058-9)
- Zang W & Walter MR 1989. Latest Proterozoic plankton from the Amadeus Basin in Central Australia. *Nature* 337: 642–645, <https://doi.org/10.1038/337642a0>.
- Zhang F, Xu H, Konishi H, Kemp JM, Roden EE & Shen Z 2012. Dissolved sulfide–catalyzed precipitation of disordered dolomite: Implications for the formation mechanism of sedimentary dolomite. *Geochimica & Cosmochimica Acta* 97: 148–165, <https://doi.org/10.1016/j.gca.2012.09.008>.
- Zhou C, Huyskens MH, Lang X, Xiao S & Yin Q–Z 2019. Calibrating the termination of Cryogenian global glaciations. *Geology* 47: 251–254, <https://doi.org/10.1130/G45719.1>.